BIOCHEMISTRY
including biophysical chemistry & molecular biology

Article

pubs.acs.org/biochemistry

The -Cys-X1-X2-Cys- Motif of Reduced Glutaredoxins Adopts a Consensus Structure That Explains the Low pK_a of Its Catalytic Cysteine

Nicolas Foloppe,*[,†] Alexios Vlamis-Gardikas,[‡] and Lennart Nilsson*[,§]

[†]51 Natal Road, Cambridge CB1 3NY, United Kingdom

[‡]Department of Chemistry, Division of Organic Chemistry, Biochemistry and Natural Products, University of Patras, Rion 26504, Greece

[§]Department of Biosciences and Nutrition, Center for Biosciences, Karolinska Institutet, S-141 83 Huddinge, Sweden

Supporting Information

ABSTRACT: The -Cys-X1-X2-Cys- active site motif is central to the function of enzymes of the thioredoxin superfamily, including glutaredoxins. Their chemistry depends on the lowered pK_a of the N-terminal thiolate cysteine of the -Cys-X1-X2-Cys- sequence; therefore its structure, dynamics, and electrostatics matter. Much information about the glutaredoxin structures was obtained by nuclear magnetic resonance (NMR), yet these various NMR structures produced heterogeneous and discordant views of the -Cys-X1-X2-Cys- motifs. This study addresses these inconsistencies by a computational and experimental investigation of three diverse reduced -Cys-X1-X2-Cys- motifs, from human glutaredoxin 1 (hGrx1), *Escherichia coli* glutaredoxin 2 (EcGrx2), and T4 virus glutaredoxin (T4Grx). The NMR models do not account for the low pK_a of the N-terminal cysteine. However, extensive investigations of the NMR conformers by simulations yielded consensus structures for the -Cys-X1-X2-Cys- motif, with well-defined orientations for the cysteines. pK_a calculations indicated that the consensus structure stabilizes the thiolate by local hydrogen bonds. The consensus structures of EcGrx2 and T4Grx formed the basis for predicting low pK_a values for their N-terminal cysteines. Subsequent experimental titrations showed that these pK_a values are <5, supporting the validity of the consensus structure. The simulations also revisited the conformational dynamics of side chains around the -Cys-X1-X2-Cys- motif, which allowed reconciliation of calculated and measured pK_a values for important hGrx1 mutants. The conformational spread of these side chains, which differs between NMR and molecular dynamics models, is likely to be relevant to substrate recognition. The new structural models determined in this work should prove to be valuable in future molecular studies of the glutaredoxins.

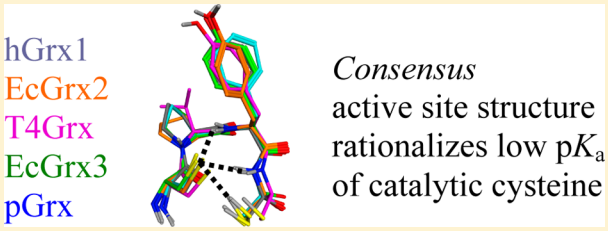

Glutaredoxins (also called thioltransferases[1]) belong to the thioredoxin superfamily of oxidoreductases,[2,3] are ubiquitous,[4] and play a general role in the maintenance and control of cellular redox homeostasis, including regulation of the level of protein glutathionylation.[1,5,6] Dithiol glutaredoxins (Grxs) contain a conserved -Cys-X1-X2-Cys- active site motif[2] that is central to the catalytic function of these enzymes and their cysteine chemistry.[1] Importantly, the N-terminal (N-ter) cysteine thiol of the glutaredoxin -Cys-X1-X2-Cys- motif has a pK_a value significantly lower than that of a free cysteine, usually $\lesssim$5.[7−10] This pK_a is a key determinant of the many cellular functions of glutaredoxins, including their reactivity and redox potentials, as recently reviewed.[1,6] The low-pK_a cysteine is primed for nucleophilic attack on disulfide substrates, initiating the thiol−disulfide exchange reactions. This leads to an intermediate mixed disulfide in which the substrate is covalently linked to the glutaredoxin. Then, a reduced substrate is released via mechanisms that are still being investigated.[1,6]

Structurally, glutaredoxins are relatively small proteins with the thioredoxin fold,[11] where the -Cys-X1-X2-Cys- active site can be oxidized (disulfide) or reduced (dithiol). Crystallographic studies of reduced glutaredoxins have proven to be challenging.[12,13] Thus, much of the experimental structural data for reduced glutaredoxins has been obtained from nuclear magnetic resonance (NMR) studies in solution, for *Escherichia coli* Grx1 (EcGrx1),[14] *E. coli* Grx2 (EcGrx2),[15] *E. coli* Grx4,[16] bacteriophage T4 Grx (T4Grx),[17] and human glutaredoxin 1 (hGrx1).[18] EcGrx2 is larger than conventional glutaredoxins, and NMR studies have revealed that it adopts an atypical architecture when compared to those of other glutaredoxins.[15] *E. coli* Grx4 is a monothiol glutaredoxin in which the second active site cysteine is replaced with a serine.[17] This study concentrates on dithiol glutaredoxins, where the active site motif sequence is frequently -Cys-Pro-Tyr-Cys- (as in EcGrx1, EcGrx2, and hGrx1), with variations such as -Cys-Val-Tyr-Cys-

Received: May 21, 2012
Revised: August 7, 2012
Published: September 11, 2012

dx.doi.org/10.1021/bi3006576 | *Biochemistry* 2012, 51, 8189−8207

in T4Grx.[17] hGrx1 has been a major model system for the investigation of glutaredoxins.[1,4,8,10]

Despite the functional importance of the -Cys-X1-X2-Cys- motif in glutaredoxins, the NMR structures of this motif are surprisingly heterogeneous for any given glutaredoxin, but are also disparate across glutaredoxins (Figure 1). This may reflect

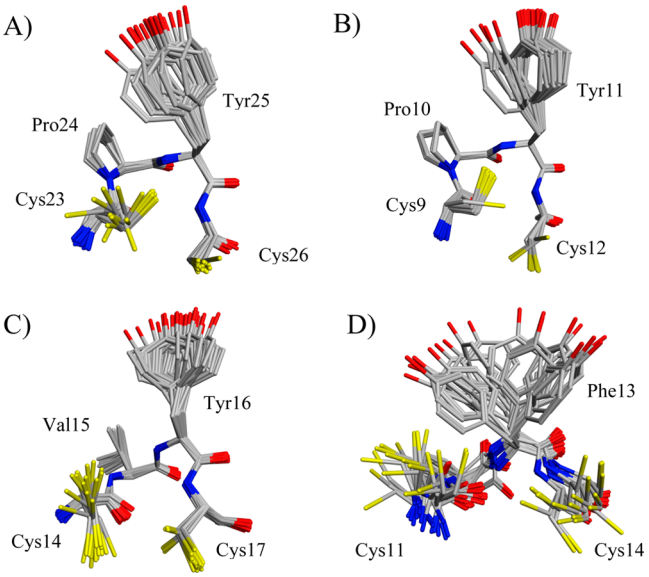

Figure 1. Conformational heterogeneity of the -Cys-X1-X2-Cys- motif in NMR structures of reduced glutaredoxins. The structures are for hGrx1 [(A) PDB entry 1JHB], EcGrx2 [(B) PDB entry 1G7O], T4Grx [(C) PDB entry 1DE2], and EcGrx1 [(D) PDB entry 1EGR]. For each protein, all conformers of the NMR model were superimposed by best fit on the backbone of the -Cys-X1-X2-Cys- active site motif, the residues of which are labeled. For the sake of clarity, hydrogens are not shown. The conformational heterogeneity of the reduced -Cys-X1-X2-Cys- motifs in the NMR structures is reflected in the various orientations of their cysteine side chains (Table 2), which relate to the hydrogen bonds stabilizing the catalytic thiolate (Table 3). The conformational spread of the NMR models contrasts with the more precise consensus conformation obtained by MD simulations (Figures 4 and 5).

actual differences between these enzymes, considering that the ability to probe the flexibility and dynamics of biomolecules in solution is considered a strength of NMR.[19−21] Structural differences between the -Cys-X1-X2-Cys- motifs could arise from sequence differences between motifs (e.g., hGrx1 vs T4Grx) or from the distinct overall protein architectures in which the motif is embedded (e.g., hGrx1 vs EcGrx2). Indeed, there is evidence that even motifs with the same sequence can adopt dissimilar conformational populations in EcGrx1 and EcGrx3.[22] This matters because the structure and dynamics of the -Cys-X1-X2-Cys- motifs strongly affect the pK_a of the nucleophilic cysteine,[9,22−25] and this pK_a is a major determinant of the redox potential of enzymes in the thioredoxin (Trx) superfamily.[3,23,24,26,27] The factors that lower the pK_a of the N-ter cysteine of the -Cys-X1-X2-Cys- motifs remain the subject of intense experimental and theoretical investigations.[9,10,22−26,28−36] Clearly, reliable structural characterization of the reduced -Cys-X1-X2-Cys- active sites is a prerequisite for understanding their chemistry and substrate recognition. Thus, one has to consider the possibility that the differences observed in the NMR models of reduced glutaredoxins may result from a lack of experimental restraints or limitations in the structure refinement protocols. For example, it was shown to be the case with catalytic Cys11 in reduced *E. coli* Grx3.[9]

Indeed, the precision and accuracy of NMR structures have been an ongoing topic of discussion.[20,37−41] Conformational spread in some regions of NMR structures may reflect a dearth of experimental restraints. It can be difficult or impossible to derive unambiguous NMR structural restraints for protein regions that quickly interconvert between conformers, such as solvent-accessible loops or side chains. In such regions, the apparent structural heterogeneity is likely to reflect a lack of suitable restraints rather than a fit to experimental data. Thus, improving and testing the refinement of NMR structural models have been concerns.[39,42,43] Progress was made by extension and optimization of the molecular force field used during refinement, particularly regarding nonbonded[44] and torsional[43,44] parameters. Also, it has become apparent that pK_a calculations can help assess and select NMR conformers.[22,31,41] The addition of explicit solvent during refinement has led to notable improvements,[22,38,40,43,44] even with short molecular dynamics (MD) simulations in a relatively thin layer of water.[40,43] Importantly, the improvement was not only in generic steric criteria for the quality of structure but also in the fit to the experimental data.[40] The benefits of MD simulations in explicit solvent were not surprising because such protocols provide a physically relevant representation of the protein, its dynamics, and protein−solvent interactions.

Extensive MD simulations can be used to probe the structure, dynamics, and electrostatics of thiol-disulfide oxidoreductases.[9,22,25,35,45] With sufficiently long simulations, the CHARMM22 force field[46] yields a well-balanced representation of the conformational dynamics of the glutaredoxin -Cys-X1-X2-Cys- motifs with a thiolate N-ter cysteine.[9,22,25] Such simulations also offer insights into the orientation and flexibility of side chains surrounding the -Cys-X1-X2-Cys- motif, with implications for their contribution to the thiolate stabilization or substrate recognition.

Here, we use extensive MD simulations in explicit solvent to clarify the structure and dynamics of reduced thiol-disulfide oxidoreductases, as illustrated with EcGrx1, EcGrx2, T4Grx, wild-type hGrx1, and two hGrx1 mutants. The conformers obtained by NMR and MD simulations are assessed via Poisson−Boltzmann-based pK_a calculations. The conformers only account for the low pK_a of the catalytic cysteine after extended MD simulation and structural reorganization of the various -Cys-X1-X2-Cys- motifs. EcGrx2, T4Grx, and hGrx1 adopt a predominant consensus conformation for their -Cys-X1-X2-Cys- motifs, where the N-ter and C-terminal (C-ter) cysteines adopt χ_1 = *trans* and χ_1 = *gauche*$^-$ conformations, respectively. In this consensus structure, the catalytic thiolate forms several hydrogen bonds that explain its stabilization. Experimental measurements confirmed the prediction that EcGrx2 and T4Grx contain a cysteine with a pK_a ≤5, contrary to the suggestion that T4Grx may be peculiar in this respect.[17] The simulations also help interpret the mutation data with hGrx1 in relation to the pK_a of its catalytic cysteine[10] and provide an overall different picture of the recognition surface around the active sites of EcGrx2 and T4Grx. Thus, the simulated structures also pave the way for an improved understanding of substrate recognition by glutaredoxins and other enzymes in the thioredoxin superfamily.

dx.doi.org/10.1021/bi3006576 | *Biochemistry* 2012, 51, 8189−8207

MATERIALS AND METHODS

Preparation of Wild-Type Reduced Proteins for Simulation. For EcGrx1, the simulations are extensions from previous work,[22] from the previous value of 75 ns to the new value of 200 ns reported here. Other MD simulations were initiated from NMR models, for hGrx1 (PDB entry 1JHB), EcGrx2 (PDB entry 1G7O), and T4Grx (PDB entry 1DE2). Details for the starting conformers are given in Table S1 and Figures S1−S3 of the Supporting Information. The starting NMR conformers differed from the consensus conformation of the reduced -Cys-X1-X2-Cys- motif that emerged after MD simulations. In these starting structures, the hydrogen bonds between the catalytic sulfur of the N-ter cysteine and the rest of the -Cys-X1-X2-Cys- motif were not formed or incompletely formed. For example, the $S^{\gamma}\cdots S^{\gamma}$ distance was usually well above that of a hydrogen bond interaction (Table S1 of the Supporting Information). This allowed us to test whether the simulations would spontaneously stabilize conformations different from those presented by the NMR models, with newly formed hydrogen bonds to the thiolate. For each protein, at least two MD simulations were performed, each starting from a different -Cys-X1-X2-Cys- conformation, to test convergence. Convergence was observed in every case. For the sake of convenience, each MD simulation was given a name (Table 1).

Table 1. Summary and Names of the MD Simulations

protein	construct[a]	MD name	MD length (ns)
hGrx1	native	*hGrx1_a*	128
	native	*hGrx1_b*	120
	mutant K20L	*hGrx1_K20L*	60
	mutant K20Q	*hGrx1_K20Q*	60
EcGrx2	native (His8 neutral)	*EcGrx2_a*	100
	native (His8 neutral)	*EcGrx2_b*	175
	native (His8 protonated)	*EcGrx2_c*	100
T4Grx	native	*T4Grx_a*	120
	native	*T4Grx_b*	140
	native	*T4Grx_c*	140
EcGrx1	native	*EcGrx1_a*	200[b]
	native	*EcGrx1_b*	200[b]

[a]All these simulations were performed for reduced forms of the active site. [b]The two simulations of EcGrx1 are extension from 75 to 200 ns of previously reported simulations.[22]

To facilitate structural comparisons, the same residue numbering as in the NMR models was kept. It is offset by 1 relative to the numbering used in a directly relevant study for hGrx1,[10] but the correspondence between the two numbering schemes is straightforward.

The titratable groups were assigned conventional protonation states at pH 7 unless stated otherwise. To the best of our knowledge, no experimental data that could help specify the protonation states of the histidines in the simulated proteins are available. Thus, all histidines were treated as neutral with a proton on $N^{\delta 1}$, including His8 of EcGrx2 in simulations *EcGrx2_a* and *EcGrx2_b*. Because His8 of EcGrx2 is in the active site, it was also treated as positively charged (proton on both $N^{\delta 1}$ and $N^{\epsilon 2}$) in simulation *EcGrx2_c*. Given general knowledge about reduced glutaredoxins,[1,3,6,9] the N-ter cysteines in the -Cys-X1-X2-Cys- motifs were treated as thiolates during the simulations. Force field parameters for the thiolate form of a cysteine were as previously described.[9,22]

Preparation of hGrx1 Mutants. Two hGrx1 mutants studied experimentally,[10] Lys20Leu and Lys20Gln, were simulated after being built from hGrx1 NMR conformer 5 (Table S1 of the Supporting Information). The mutated side chains were built using the conformation of Lys20 as a template for the counterpart atoms in Leu20 or Gln20. The amide group of Gln20 was oriented initially to make hydrogen bonds with Cys23 and Thr22. Then, the mutated side chains were energy-minimized keeping the rest of the protein fixed. The MD simulations for the hGrx1 mutants were prepared and performed as with the wild type.

Molecular Dynamics Protocols. Energy minimizations and MD simulations were performed with CHARMM,[47] following a previously described protocol.[22,25] It uses the CHARMM protein force field,[46] a dielectric constant of 1.0, and atom-based nonbonded interactions truncated beyond 12 Å with a force shift,[48] known to provide a satisfactory treatment of electrostatics.[49−51] Nonbonded lists were maintained to 14 Å and updated heuristically. Graphical operations and structural overlays were performed with MOE.[52]

All simulations were performed with periodic boundary conditions in cubic boxes of solvent, the size of which depended on the protein and allowed for ample solvation with respect to the nonbonded cutoffs. Each protein was overlaid with a box of pre-equilibrated TIP3P water,[53] and the waters with their oxygen atom <2.7 Å from any protein atom were removed. It was checked graphically that no water molecule was accidentally trapped in the core of a protein. When needed, each system was neutralized with chlorine or sodium counterions. Covalent bonds involving a hydrogen were constrained with SHAKE.[54]

Then, the solvent was energy minimized keeping the protein fixed. In a second round of energy minimization, both the solvent and the protein were allowed to relax. Each system was then subjected to MD simulations, using the leapfrog integrator and a 0.002 ps time step. Heating to 300 K was performed in 6 ps, with the protein atoms harmonically constrained to their initial position with a force constant of 2.0 kcal mol^{-1} $Å^{-2}$. Each simulation was pursued at 300 K in the *NVT* ensemble for 40 ps, with the constraints on the protein kept during the first 20 ps only. This was followed by 20 ps of MD in the *NPT* ensemble, to monitor possible volume changes. The primary box volume changed only very slightly upon simulation at a constant pressure, indicating that the number of water molecules present was reasonable. The MD simulations were then continued in the *NVT* ensemble, for the lengths of time listed in Table 1.

pK_a Calculations. The pK_a values of the protein titratable groups were calculated by solving the Poisson−Boltzmann equation with continuum dielectrics, using a protocol that performed satisfactorily with cysteine residues in comparable systems.[9,22,25] With the NMR conformers, the pK_a values were calculated using the coordinates deposited in the PDB. With the MD simulations, the pK_a values were calculated on snapshots extracted every 200 ps. The electrostatic calculations were performed with UHBD,[55] without any explicit solvent molecules, and using the parameters of a validated protocol.[56,57] This protocol uses a modified OPLS parameter set to assign partial charges and van der Waals radii and includes only polar hydrogens. Reference pK_a values of the model compounds corresponding to the titrated groups were 4.0 for Asp, 12.0 for Arg, 8.3 for Cys, 4.4 for Glu, 6.3 for His, 10.4 for Lys, 9.6 for Tyr, 7.5 for the N-ter amino group, and 3.8 for the C-ter

dx.doi.org/10.1021/bi3006576 | *Biochemistry* 2012, 51, 8189−8207

Table 2. Conformation of the Cysteine Side Chains[a] of the Reduced -Cys-X1-X2-Cys- Motif in Glutaredoxins

		NMR models								
		N-ter Cys					C-ter Cys			
			no. of χ_1 conformers					no. of χ_1 conformers		
	PDB entry	residue	g^+	g^-	*trans*	other	residue	g^+	g^-	*trans*	other
hGrx1	1JHB	Cys23	0	6	10	4	Cys26	0	20	0	0
EcGrx2	1J7O	Cys9	0	0	0	21	Cys12	3	0	0	18
T4Grx	1DE2	Cys14	16	2	0	12	Cys17	4	3	19	4
EcGrx1	1EGR	Cys11	0	10	10	0	Cys14	0	17	3	0
		MD simulation models								
		N-ter Cys					C-ter Cys			
			percent of χ_1 conformers					percent of χ_1 conformers		
	trajectory	residue	g^+	g^-	*trans*	other	residue	g^+	g^-	*trans*	other
hGrx1	*hGrx1_a*	Cys23	0.0	0.1	99.6	0.3	Cys26	0.0	99.9	0.0	0.1
	hGrx1_b	Cys23	4.2	6.0	88.9	0.9	Cys26	0.0	99.9	0.0	0.1
	hGrx1_K20L	Cys23	0.0	0.0	99.7	0.3	Cys26	0.0	99.9	0.0	0.1
	hGrx1_K20Q	Cys23	0.0	0.6	99.0	0.4	Cys26	0.0	99.9	0.0	0.1
EcGrx2	*EcGrx2_a*	Cys9	6.5	0.0	93.4	0.1	Cys12	0.0	99.9	0.0	0.1
	EcGrx2_b	Cys9	0.1	0.7	98.9	0.3	Cys12	11.1	87.2	0.0	1.7
	EcGrx2_c	Cys9	3.7	8.6	87.3	0.4	Cys12	0.0	96.0	4.0	0.0
T4Grx	*T4Grx_a*	Cys14	0.0	0.0	98.2	1.8	Cys17	0.0	98.1	1.7	0.2
	T4Grx_b	Cys14	0.3	13.3	82.7	3.7	Cys17	0.0	79.4	19.0	1.6
	T4Grx_c	Cys14	14.7	0.1	83.2	2.0	Cys17	0.0	86.0	13.0	1.0
EcGrx1	*EcGrx1_a*	Cys11	45.7	4.8	48.9	0.6	Cys14	0.0	96.4	3.2	0.4
	EcGrx1_b	Cys11	69.4	5.8	24.0	0.8	Cys14	0.0	96.2	3.2	0.6

[a]Analyzed in terms of the side chain χ_1 torsion angles.

carboxyl group. The solvent dielectric constant was 78.5, and the protein dielectric constant (ϵ_P) was set to 3.0 because this value has yielded reasonable results with comparable systems.[9,22,25]

The electrostatic potentials were calculated using the grid focusing technique,[58] using four successive cubic grids; the smallest grid was 20 Å^3 with a 0.25 Å spacing. The linearized Poisson−Boltzmann equation was solved at a temperature of 298 K, with an ionic strength of 150 mM, and with an ion exclusion (Stern) layer of 2.0 Å. The titration curves were calculated using the cluster method implemented in Hybrid.[59]

Structural Analysis. We follow the standard recommendation for structural descriptions.[60] For torsions, the *gauche* minus (g^-) and *gauche* plus (g^+) ranges are defined as $-60 \pm 30°$ and $60 \pm 30°$, respectively.

A distance cutoff of 4.0 Å between sulfur and hydrogen bond donor D was used for identification of a hydrogen bond, consistent with previous studies.[22,61−65] The additional angular conditions (S···H−D $\geq$ 120.0° and C−S···H $\geq$ 70.0°) were applied for the corresponding hydrogen bond to be considered formed.

Purification of Recombinant Glutaredoxins. The sequence encoding T4Grx (PDB entry 1DE2) was optimized for expression in *E. coli* and cloned in an overexpression vector by DNA 2.0. The synthetic gene sequence encoded an additional six-histidine tag at the N-terminus of the protein and a thrombin cleavage site immediately after it. After treatment with thrombin, T4Grx would start as GSHM, with M being the initiator methionine of the wild-type protein. BL21(DE3) cells transformed with the plasmid obtained from DNA 2.0 were grown in rich medium to autoinduce expression of T4Grx.[66] After 24 h at 250 rpm and 18 °C, cells were harvested and resuspended in 20 mM potassium phosphate (pH 7.4). Lysozyme (0.5 mg/mL) and DNase I (0.05 mg/mL) were added, and the sample was kept on ice for 1 h, after which it was sonicated. KCl (250 mM), Triton X-100 (1%), and imidazole (20 mM) were added; the sample was centrifuged at 15000*g* for 30 min at 4 °C, and the supernatant was chromatographed on a HisTrap FF column (GE Healthcare) in 20 mM potassium phosphate, 250 mM KCl, and 20 mM imidazole (pH 7.4) at 4 °C. Bound T4Grx was eluted in a gradient of imidazole up to 500 mM in the same buffer. The most pure samples (as judged by sodium dodecyl sulfate−polyacrylamide gel electrophoresis) were concentrated, treated with thrombin (0.1 unit/mg of protein, 3 h at room temperature), reduced with DTT (5 mM, 30 min at room temperature), and chromatographed on Sephadex G-50 superfine in 20 mM Tris-HCl, 100 mM KCl, and 1 mM EDTA (pH 8.0) at 4 °C. T4Grx was obtained in a homogeneous form after this purification step. The molar extinction coefficient at A_{280} used to calculate the concentration of purified protein was 5960 M^{-1} cm^{-1}.

E. coli Grx2 (~0.3 mM) was purified to homogeneity as previously described.[67] A molar extinction coefficient of 21860 M^{-1} cm^{-1} at A_{280} was used for EcGrx2.

Measurement of the Concentration of the Thiolate Anions in EcGrx2 and T4Grx. Measurements of the thiolate anion were performed at A_{240}.[68,69] Changes in the ionization state of the thiolate at different pH values were followed by the A_{240}/A_{280} ratio. In short, glutaredoxins at high concentrations (0.3−0.5 mM) were initially reduced in excess (10 mM) DTT in 20 mM Tris-HCl and 1 mM EDTA (pH 8) for 30 min at room temperature. DTT was removed by chromatographing EcGrx2 in 20 mM potassium phosphate and 1 mM EDTA (pH 7.0) through a Sephadex G-50 superfine column. T4Grx was desalted in 20 mM potassium phosphate and 1 mM EDTA (pH

dx.doi.org/10.1021/bi3006576 | *Biochemistry* 2012, 51, 8189−8207

Table 3. Hydrogen Bonds between the Active Site N-ter Cysteine Sulfur and the -Cys-X1-X2-Cys- Motif

	acceptor···donor[a]	NMR[b]	MD[c]			
hGrx1		1JHB	*hGrx1_a*	*hGrx1_b*	*hGrx1_K20L*	*hGrx1_K20Q*
	$S^{\gamma}_{23}\cdots N_{25}$	13 (65.0%)	90.6	85.2	95.5	90.9
	$S^{\gamma}_{23}\cdots N_{26}$	12 (60.0%)	63.4	60.4	79.4	63.0
	$S^{\gamma}_{23}\cdots S^{\gamma}_{26}$	14 (70.0%)	29.0	27.9	39.4	32.2
EcGrx2		1J7O	*EcGrx2_a*	*EcGrx2_b*	*EcGrx2_c*	
	$S^{\gamma}_{9}\cdots N_{11}$	19 (90.5%)	80.5	74.2	67.5	
	$S^{\gamma}_{9}\cdots N_{12}$	15 (71.4%)	60.4	54.9	50.1	
	$S^{\gamma}_{9}\cdots S^{\gamma}_{12}$	0 (0.0%)	45.6	44.7	43.3	
T4Grx		1DE2	*T4Grx_a*	*T4Grx_b*	*T4Grx_c*	
	$S^{\gamma}_{14}\cdots N_{16}$	0 (0.0%)	75.0	53.9	68.7	
	$S^{\gamma}_{14}\cdots N_{17}$	0 (0.0%)	79.5	63.5	81.7	
	$S^{\gamma}_{14}\cdots S^{\gamma}_{17}$	0 (0.0%)	67.8	45.0	54.9	
EcGrx1		1EGR	*EcGrx1_a*	*EcGrx1_b*		
	$S^{\gamma}_{11}\cdots N_{13}$	1 (5.0%)	55.2	51.3		
	$S^{\gamma}_{11}\cdots N_{14}$	0 (0.0%)	63.0	72.7		
	$S^{\gamma}_{11}\cdots S^{\gamma}_{14}$	0 (0.0%)	61.9	71.0		

[a]Possible hydrogen bonds between the sulfur of the N-terminal cysteine S^{γ} and hydrogen bond donors in the -Cys-X1-X2-Cys- motif; the subscript indicates the residue number. [b]Frequency of occurrence of each hydrogen bond in the NMR structures (the PDB entry codes are given), as the number of conformers where the hydrogen bond is observed, and the corresponding percentage relative to the total number of NMR conformers. [c]Frequency of occurrence of each hydrogen bond during the MD simulations (each MD identifier is given), in percent of the time. The geometric criteria used to define the presence of a hydrogen bond are given in Materials and Methods.

6.0). The reduction state of the obtained glutaredoxins was assessed by the DTNB assay[70] measuring total reduced thiols. The DTT-free samples (0.2−0.4 mM) were kept on ice and served as a source of protein for the titrations in buffers with different pH values. The reduced stocks were diluted (1:15 to 1:40) in the desired pH buffer to a final concentration that would give a reasonable A_{280} for measurements (~7 μM EcGrx2 gave an A_{280} of 0.15; ~14 μM T4Grx gave an A_{280} of ~0.1). Any scattering was corrected by subtracting A_{310} from the A_{240} and A_{280} values. For each A_{240} and A_{280} measurement, full spectra were recorded from 210 to 340 nm at 25 °C, against 20 mM potassium phosphate and 1 mM EDTA (pH 7.0 for EcGrx2 and pH 6.0 for T4Grx), diluted in the respective pH buffers of the titration. The buffer concentration for all pH buffers was between 100 and 150 mM with the pH ranging from 2.71 to 10.04 as determined by a pH meter. Measurements started immediately after the dilution of the samples in the pH buffers. The path length of the cuvettes used was 1 cm. No visible precipitation or increase in A_{310} was observed in any of the these measurements, consistent with the complete solubility of EcGrx2 and T4Grx during the wavelength scans. There was no oxidation of the reduced stocks of glutaredoxins on ice as assessed by the DTNB assay over a period of at least 3 h.

The titrations in the low-pH region (pH <7.5) were analyzed by nonlinear regression fitting of the data (A_{240}/A_{280}) to a sigmoidal logistic dose−response model (other sigmoidal models gave equivalent results) with Origin 7 from OriginLab. The inflection point of the fitted sigmoidal model was used to estimate the corresponding pK_a (T4Grx) or a higher bound for the pK_a if the titration curve was incomplete at the lowest extreme of pH (EcGrx2).

RESULTS AND DISCUSSION

Table 1 summarizes the systems investigated and the performed MD simulations. A detailed analysis of the reduced active site of EcGrx1 was already presented,[22] but these simulations have been extended here for additional comparisons with other glutaredoxins. In the following, we identify the cysteines of the -Cys-X1-X2-Cys- motif simply as the N-ter and C-ter cysteines. When this generic terminology is not sufficient, we use the same individual residue numbers as in the structures deposited in the PDB (Table 2). hGrx1 and EcGrx2 active sites contain conventional glutaredoxin motif sequences, -Cys23-Pro24-Tyr25-Cys26- and -Cys9-Pro10-Tyr11-Cys12-, respectively, yet the tertiary architecture of EcGrx2 is atypical for a glutaredoxin.[15,67] T4Grx contains the atypical glutaredoxin sequence -Cys14-Val15-Tyr16-Cys17-.

The computational analyses were performed before the experimental measurements, which were directed following the computational predictions. To reflect this approach, we present and discuss the computational results before the experimental data obtained to test the predictions. However, we start with a detailed comparison of the NMR models used as starting points for our investigations.

Structural Heterogeneity of the NMR Models of the Reduced Active Sites. *Conformations of the Active Site Cysteine Side Chains.* This section summarizes the structural pictures of glutaredoxin reduced active sites as they appear in the NMR structures (Figure 1) of hGrx1 (PDB entry 1JHB[18]), EcGrx2 (PDB entry 1G7O[15]), T4Grx (PDB entry 1DE2[17]), and EcGrx1 (PDB entry 1EGR[14]). Figure 1 shows that the NMR models are heterogeneous with respect to the orientations of the active site cysteines, within and across models. This is confirmed when the χ_1 torsion angles of these cysteine side chains are scrutinized (Table 2). These conformations are critical because they control the detailed interactions between the cysteine thiol groups and the rest of the protein,[9,22,25] in particular the hydrogen bonds involving the N-ter cysteine sulfur S^{γ}, which can stabilize its thiolate form.[9,22,25,28,30]

For the χ_1 torsion of the N-ter cysteine, no clear conformational preference emerges from the NMR structures. With hGrx1 and EcGrx1, the N-ter cysteine is mostly in g^- and *trans*. With EcGrx2, the N-ter cysteine falls outside the conventional *gauche* or *trans* rotamers, i.e., in the "other"

dx.doi.org/10.1021/bi3006576 | *Biochemistry* 2012, 51, 8189−8207

Table 4. Calculated pK_a Values of the Reduced Cysteines in the -Cys-X1-X2-Cys- Motif in Glutaredoxins

		N-ter Cys		C-ter Cys	
		NMR models			
	PDB entry	residue	average pK_a ± SD	residue	average pK_a ± SD
hGrx1	1JHB	Cys23	6.9 ± 1.8	Cys26	14.0 ± 1.1
EcGrx2	1J7O	Cys9	8.3 ± 1.3	Cys12	15.2 ± 2.4
T4Grx	1DE2	Cys14	13.3 ± 2.6	Cys17	13.8 ± 3.0
EcGrx1	1EGR	Cys11	10.1 ± 1.9	Cys14	15.2 ± 2.9
		MD simulation models			
	trajectory	residue	average pK_a ± SD	residue	average pK_a ± SD
hGrx1	*hGrx1_a*	Cys23	5.4 ± 0.9	Cys26	15.1 ± 1.4
	hGrx1_b	Cys23	5.8 ± 1.0	Cys26	14.6 ± 1.4
	hGrx1_K20L	Cys23	5.4 ± 0.9	Cys26	15.6 ± 1.2
	hGrx1_K20Q	Cys23	5.7 ± 0.9	Cys26	15.1 ± 1.3
EcGrx2	*EcGrx2_a*	Cys9	5.5 ± 0.9	Cys12	13.8 ± 1.3
	EcGrx2_b	Cys9	5.1 ± 1.0	Cys12	13.7 ± 1.5
	EcGrx2_c[a]	Cys9	5.5 ± 1.4	Cys12	13.5 ± 2.1
T4Grx	*T4Grx_a*	Cys14	5.2 ± 1.3	Cys17	15.7 ± 1.5
	T4Grx_b	Cys14	5.9 ± 1.6	Cys17	14.8 ± 2.1
	T4Grx_c	Cys14	5.2 ± 1.5	Cys17	15.8 ± 1.8
EcGrx1	*EcGrx1_a*	Cys11	5.0 ± 0.6	Cys14	17.0 ± 0.5
	EcGrx1_b	Cys11	4.8 ± 0.3	Cys14	17.3 ± 0.3

[a]*EcGrx2_c* was obtained with His8 protonated, while His8 was neutral in simulations *EcGrx2_a* and *EcGrx2_b*. SD: Standard Deviation.

range. This noncanonical conformation was intriguing, especially because it might somehow reflect the atypical structural character of EcGrx2.[15,67] Yet, with T4Grx, almost half of the NMR conformers of the N-ter cysteine are also in the other range while the majority are in g^+.

The NMR conformers also present a heterogeneous view of the C-ter cysteine orientation (Figure 1 and Table 2), analyzed with respect to its χ_1 torsion. While only the g^- rotamer is populated in hGrx1, it is not occupied in EcGrx2. In EcGrx2, the other and g^+ ranges are the most populated. In T4Grx, the C-ter cysteine occupies the g^+, g^-, *trans*, and other ranges, with a major population in *trans*. In contrast, g^- is predominantly populated by the C-ter cysteine in the NMR structure of EcGrx1. Overall, it is clear that the NMR models display a conformationally heterogeneous view of the active sites of reduced glutaredoxins. This is surprising, considering the homology of structure and function between these enzymes.

Hydrogen Bonds to the Sulfur of the N-ter Active Site Cysteine. The conformational heterogeneity observed in the NMR structures affects the interactions involving the catalytic N-ter cysteine, in particular the hydrogen bonds to its sulfur. Table 3 lists the hydrogen bonds formed between the N-ter cysteine accepting sulfur S^{γ}_i and hydrogen bond donors in the -Cys-X1-X2-Cys- motif. These donors include the backbone amide NH groups of residue X2 ($S^{\gamma}_i \cdots N_{i+2}$) and of the C-ter cysteine ($S^{\gamma}_i \cdots N_{i+3}$). They also include the thiol SH group of the C-ter cysteine ($S^{\gamma}_i \cdots S^{\gamma}_{i+3}$), as documented.[9,28,30,63,64,71]

In the NMR structure of hGrx1, the $S^{\gamma}_{23} \cdots N_{25}$, $S^{\gamma}_{23} \cdots N_{26}$, and $S^{\gamma}_{23} \cdots S^{\gamma}_{26}$ hydrogen bonds are formed in a majority of conformers, maybe reflecting the refinement of this structure with a thiolate sulfur for Cys23.[18] In the NMR structure of EcGrx2, only the $S^{\gamma}_9 \cdots N_{11}$ and $S^{\gamma}_9 \cdots N_{12}$ hydrogen bonds are formed in a majority of conformers, while the $S^{\gamma}_9 \cdots S^{\gamma}_{12}$ hydrogen bond is never formed. In the NMR models of T4Grx, neither the $S^{\gamma} \cdots N$ nor the $S^{\gamma} \cdots S^{\gamma}$ hydrogen bonds are formed (Table 3). This absence of hydrogen bonds that could stabilize the thiolate of Cys14 in T4Grx contrasts sharply with the results obtained after MD simulations (see section on Conformational Focusing of the T4Grx Active Site via MD Simulations), reminiscent of the situation regarding EcGrx1.[22] An analysis of the NMR structure of reduced EcGrx1 indicated that its active site conformation was inconsistent with the low pK_a of its active site N-ter cysteine and, therefore, the chemistry of this enzyme. When calculated on the basis of NMR conformers, this pK_a was much higher than that observed experimentally,[22] a strong indication that the underlying NMR structure required further refinement. Thus, pK_a calculations have emerged as a key test of structural models of the active sites in the glutaredoxin family of enzymes.[9,22]

Calculated pK_a Values as a Test of the NMR Models. The pK_a calculations used a thoroughly tested protocol,[9,56] relying on electrostatics calculated with the Poisson–Boltzmann approach, and known to perform well with glutaredoxins.[9,22,25] The pK_a values thus calculated are sensitive to some parameters, in particular the protein dielectric constant ε_P. We continue to use an ε_P of 3, because it yielded reasonable and interpretable results in previous studies.[9,22,25,56] The dependence of the calculated pK_a values on such parameters does not prevent the pK_a calculations to be an acute test of the underlying structural models, because the calculated pK_a values strongly depend on the underlying structural model.[9,22,25,41] This allows discrimination of structural models that stabilize the thiolate from those that do not. In particular, it has been argued that hydrogen bonds to the sulfur are key to stabilizing its thiolate and lowering the corresponding pK_a.[9,22,25,33,73]

The average calculated pK_a values for the N-ter cysteine in the NMR conformers are listed in Table 4; the values for the individual conformers are given in the Supporting Information (Table S2 for hGrx1, Table S3 for EcGrx2, and Table S4 for T4Grx). On the basis of the NMR conformers, the average calculated pK_a for the N-ter cysteine is >8 for EcGrx2 and T4Grx, inconsistent with the thiolate form of this cysteine at neutral pH. The NMR conformers of T4Grx are those that would destabilize the thiolate the most, with an average

dx.doi.org/10.1021/bi3006576 | *Biochemistry* 2012, 51, 8189–8207

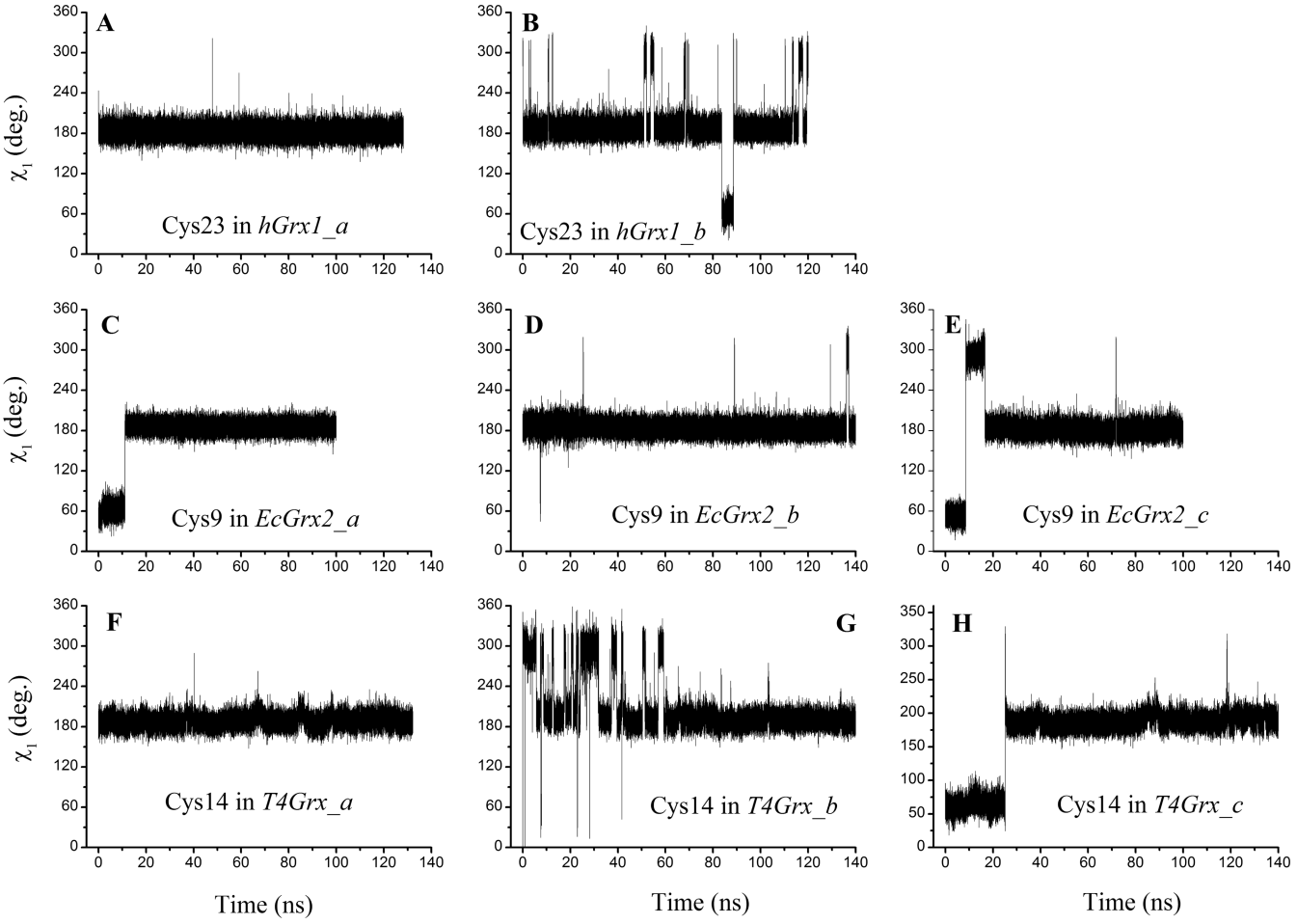

Figure 2. Conformation of the active site N-ter cysteine of the -Cys-X1-X2-Cys- motif in reduced glutaredoxins. Each panel corresponds to a different simulation, where the conformation of the active site N-ter cysteine is represented by the χ_1 torsion angle for this side chain vs time. The cysteine number and simulation name are as follows: (A) Cys23 in *hGrx1_a*, (B) Cys23 in *hGrx_b*, (C) Cys9 in *EcGrx2_a*, (D) Cys9 in *EcGrx2_b*, (E) Cys9 in *EcGrx2_c*, (F) Cys14 in *T4Grx_a*, (G) Cys14 in *T4Grx_b*, and (H) Cys14 in *T4Grx_c*. The simulation names are defined in Table 1. These plots show that χ_1 of the N-ter cysteine adopts predominantly a *trans* orientation across the studied glutaredoxins, even though the simulations were generally started with χ_1 in a different orientation (Table S1 of the Supporting Information). Importantly, the χ_1 = *trans* conformation is key for the formation of hydrogen bonds between the cysteine sulfur and the protein backbone amide NH groups, which stabilize the thiolate form of the N-ter active site cysteine.

calculated pK_a of 13.3 for Cys14, significantly higher than the pK_a of a cysteine free in solution (~8.6[74]). As with EcGrx1,[22] these high calculated pK_a values for T4Grx most likely reflect the lack of hydrogen bonds stabilizing the thiolate in the NMR conformers (Table 3 and section Hydrogen Bonds to the Sulfur of the N-ter Active Site Cysteine). Indeed, these hydrogen bonds are more frequently formed in the NMR conformers of hGrx1, leading to a lower average calculated pK_a of 6.9 for its Cys23. However, this pK_a remains significantly higher than its experimental value, reported to be 3.7 (triple-mutant construct TM-Grx[10]) or 4.2 (single-cysteine construct SC-Grx[10]) using the pH dependence of the inactivation of the enzyme by iodoacetamide.

With the NMR conformers of EcGrx2, the average calculated pK_a of 8.3 for Cys9 is also much higher than that estimated experimentally here (see section on Experimental pKa Determinations for the Cysteines in EcGrx2 and T4Grx), despite hydrogen bonds between the sulfur of Cys9 and the backbone amide NH groups of the -Cys9-Pro10-Tyr11-Cys12- motif. This is only a superficial contradiction because experiments and theoretical analyses[9,22,25,28,30] have shown that hydrogen bonding with the thiol of the active site C-ter cysteine is also important for stabilization of the N-ter cysteine thiolate. This requires that the C-ter cysteine side chain χ_1 torsion adopt a g^- orientation, which is not the case in the NMR conformers of reduced EcGrx2 (Figure 1 and Table 2). Thus, Cys12 cannot form a hydrogen bond with the Cys9 sulfur in the NMR models of EcGrx2.

Overall, the calculated pK_a values for the active site N-ter cysteine in the NMR models of hGrx1, EcGrx2, and T4Grx are significantly higher than expected on the basis of their biochemistry. This suggests that the structural models of these active sites are inconsistent with the chemistry of these enzymes and require further refinement. However, when such an assessment is made, it is important to keep in mind possible inaccuracies in the calculated pK_a values. If the calculated pK_a values were very unreliable, they could not be used to comment on the plausibility of the underlying conformers. Previous experience with the present pK_a calculation protocol has shown that it performs satisfactorily for the cysteines in the glutaredoxin active sites.[9,22,25] In addition, the difference between the pK_a values calculated for the NMR conformers

dx.doi.org/10.1021/bi3006576 | *Biochemistry* 2012, 51, 8189−8207

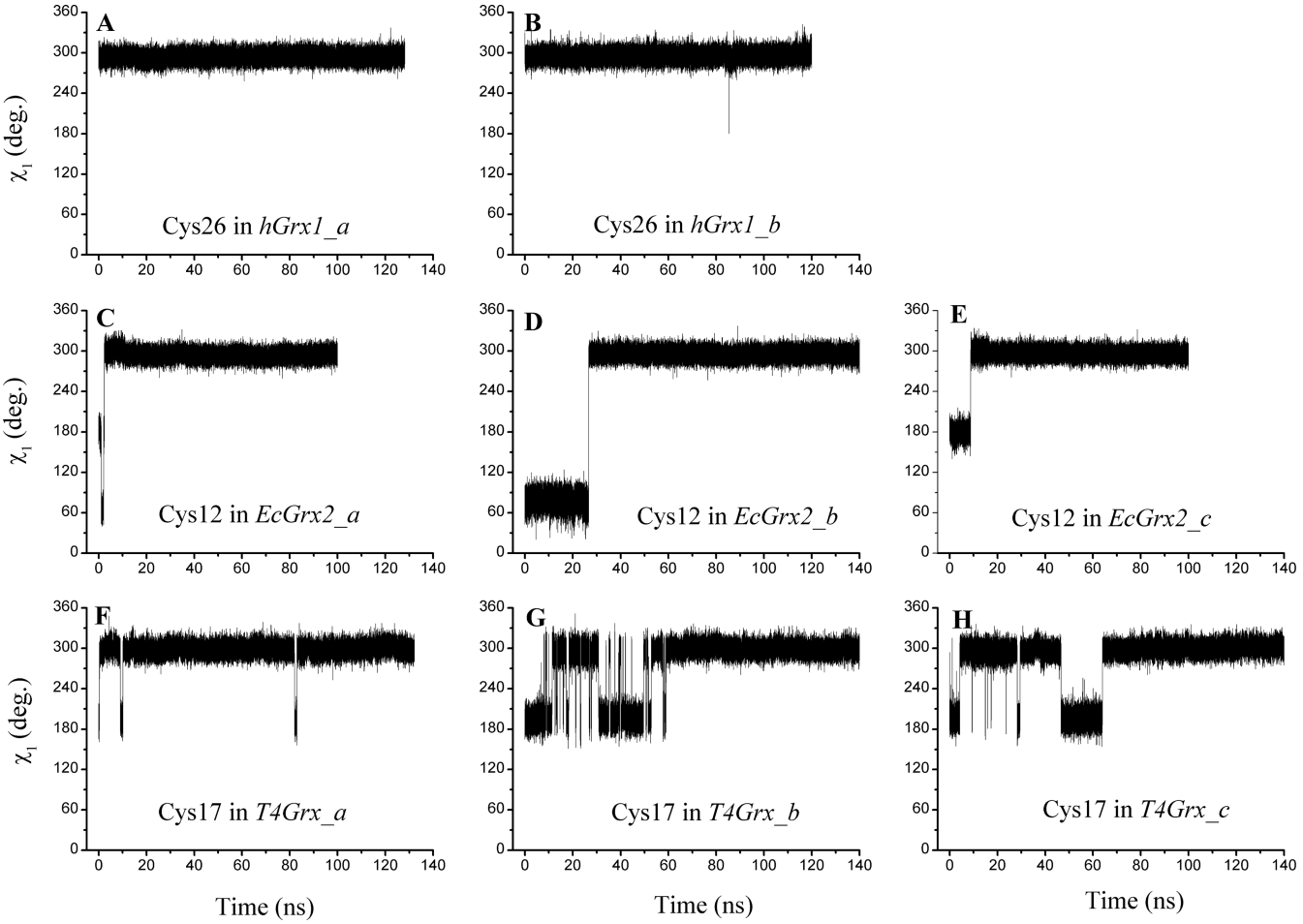

Figure 3. Conformation of the active site C-ter cysteine of the -Cys-X1-X2-Cys- motif in reduced glutaredoxins. Each panel corresponds to a different simulation, where the conformation of the active site C-ter cysteine is represented by the χ_1 torsion angle for this side chain vs time. The cysteine number and simulation name are as follows: (A) Cys26 in *hGrx1_a*, (B) Cys26 in *hGrx_b*, (C) Cys12 in *EcGrx2_a*, (D) Cys12 in *EcGrx2_b*, (E) Cys12 in *EcGrx2_c*, (F) Cys17 in *T4Grx_a*, (G) Cys17 in *T4Grx_b*, and (H) Cys17 in *T4Grx_c*. The simulation names are defined in Table 1. These plots show that χ_1 of the C-ter cysteine adopts predominantly a g^- orientation across the studied glutaredoxins, even though the simulations were started with χ_1 in a different orientation (Table S1 of the Supporting Information). The $\chi_1 = g^-$ conformation allows the formation of a hydrogen bond between the N-ter cysteine sulfur and the thiol group of the C-ter cysteine, contributing to the stabilization of the thiolate of the N-ter cysteine.

and their experimental counterpart is large (see measured pK_a values below). Thus, it is reasonable to use the calculated pK_a values to question the NMR conformers in this context. Yet, the main argument that led to the revisitation of the structure of the reduced active sites of the glutaredoxins was their behavior in MD simulations. Indeed, after application of MD simulations, the NMR models underwent systematic structural adjustements, which led to a consensus structure for the -Cys-X1-X2-Cys- motif and much lower calculated pK_a values for the N-ter active site cysteines, in tune with the biochemistry of these enzymes.

MD Simulations Provide a Different and Functionally Relevant Picture of the Glutaredoxin Reduced Active Sites. *Strategy.* The analysis of the NMR models described above indicates that they are neither a precise nor an accurate representation of the reduced active sites. The questionable aspect of these models is not their overall fold, but rather the local conformations and populations of the active sites. Hence, the NMR models provide a reasonable basis for further refinement by MD simulations with explicit solvent. Thus, extensive MD simulations were performed on hGrx1, EcGrx2, T4Grx, and EcGrx1, all in the reduced state (Table 1). For each protein, at least two simulations were performed. The previously discussed[22] simulations of EcGrx1 were extended to 200 ns to further probe the dynamics of EcGrx1 because an initial analysis[22] suggested that its active site is atypically flexible. In total, we report here more than 1 μs of MD simulations to probe the active site of reduced glutaredoxins (Table 1).

The simulations were initiated from NMR conformers (details in Table S1 of the Supporting Information), which were selected such that they had minimal hydrogen bonding to the sulfur of the N-ter cysteine. For instance, the $S^\gamma \cdots S^\gamma$ distances between the sulfur atoms of the N-ter and C-ter cysteines were typically longer than a hydrogen bond distance. The only NMR structure refined with its N-ter cysteine as a thiolate was hGrx1,[18] but the N-ter cysteine was simulated as a thiolate with all proteins investigated here, consistent with the biochemistry of these enzymes.[1,2,6] This allowed testing if additional and/or new interactions stabilizing the thiolate were formed during the MD simulations. When possible, the starting conformers were selected to differ in the relative orientations of

dx.doi.org/10.1021/bi3006576 | *Biochemistry* 2012, 51, 8189−8207

the N-ter and C-ter cysteine side chains, to test for convergence of the simulated structures. Analysis of the simulations also addresses the role of cationic side chains in stabilizing the thiolate because this has been a topic of discussion.[3,10,17]

The next four sections describe the MD refinements for each protein active site, with emphasis on the catalytic cysteines. The time course of their conformations is shown in Figures 2 (N-ter cysteine) and 3 (C-ter cysteine). Table 2 recapitulates the simulated conformational populations for these cysteines, and Table 3 summarizes their hydrogen bonding pattern. The simulated snapshots were used to calculate the pK_a values of the N-ter and C-ter cysteine every 200 ps (Table 4 and Figure 6), which are interpreted in light of the structures.

MD Refinement of Reduced hGrx1. We examine simulations *hGrx1_a* and *hGrx1_b*. Both simulations were initiated with χ_1^{Cys23} outside the *trans* range (Table S1 and Figure S1 of the Supporting Information), and χ_1^{Cys26} in g^- (as is the case in all NMR conformers). Early in simulations *hGrx1_a* and *hGrx1_b*, χ_1^{Cys23} switched to *trans* (Figure 2 and Table 2), which afterward remained populated most of the time (99.6% in *hGrx1_a* and 88.9% in *hGrx1_b*). This orientation of the N-ter cysteine allows the frequent formation of $S^{\gamma}_{23}\cdots N_{25}$ and $S^{\gamma}_{23}\cdots N_{26}$ hydrogen bonds with the backbone amides (Table 3). As a result of the reorientation of χ_1^{Cys23}, the $S^{\gamma}_{23}\cdots N_{25}$ hydrogen bond was formed significantly more frequently in the MD conformers than in their NMR counterparts (Figure 4A). The C-ter Cys26 remained in g^- during the simulations, consistent with the NMR models. This orientation allows the formation of a thiol−thiolate hydrogen bond ($S^{\gamma}_{23}\cdots S^{\gamma}_{26}$). The conformation emerging from the simulations for the -Cys23-Pro24-Tyr25-Cys26- motif reflects convergence across *hGrx1_a* and *hGrx1_b* and represents a consensus structure echoed by other -Cys-X1-X2-Cys- motifs in other glutaredoxins (Figure 5).

This convergence of simulations *hGrx1_a* and *hGrx1_b* toward similar active site structures was reflected in similar average calculated pK_a values for Cys23: 5.4 ± 0.9 in *hGrx1_a* and 5.8 ± 1.0 in *hGrx1_b* (Table 4 and Figure 6). These values are consistent with the experimentally measured pK_a of Cys23 of ∼3.7−4.2.[10] The calculated pK_a absolute value is sensitive to the protein dielectric constant ε_P. For this type of active site, a lower ε_P of 2 yields a lower pK_a value for the N-ter cysteine.[25] Indeed, the average pK_a of Cys23 calculated with an ε_P of 2 along simulation *hGrx1_a* has a value of 4.2 ± 1.4, in closer agreement with experiment.[10] However, this work aims to compare pK_a values across various glutaredoxin active sites using a consistent protocol. For these relative comparisons, an exact fit of the calculated pK_a values to experiment is not required, and we continue to report pK_a values calculated with an ε_P of 3, allowing for direct comparison with previous work.[9,22,25] Importantly, the pK_a of Cys23 calculated on the basis of the MD conformers was closer to experiment than the average pK_a of 6.9 ± 1.8 computed with the NMR conformers. This provides a strong indication that the structure of reduced hGrx1 refined by MD simulations provides a chemically more accurate picture than the NMR conformers. This theme recurred with EcGrx2 and T4Grx (see below).

In particular, the simulations suggest that the g^- conformer of Cys23 should be given less weight than in the NMR model. In the g^- conformer, the sulfur of Cys23 is turned away from the active site, toward the solvent, and cannot form a hydrogen bond to the backbone NH dipoles of the -Cys23-Pro24-Tyr25-Cys26- motif or the SH thiol of the C-ter cysteine. Thus, the g^- orientation prevents Cys23 from forming the key hydrogen bonds that stabilize its thiolate, reflected in the relatively high average pK_a calculated for Cys23 with the NMR conformers. In simulated hGrx1, the thiolate-stabilizing hydrogen bonds are

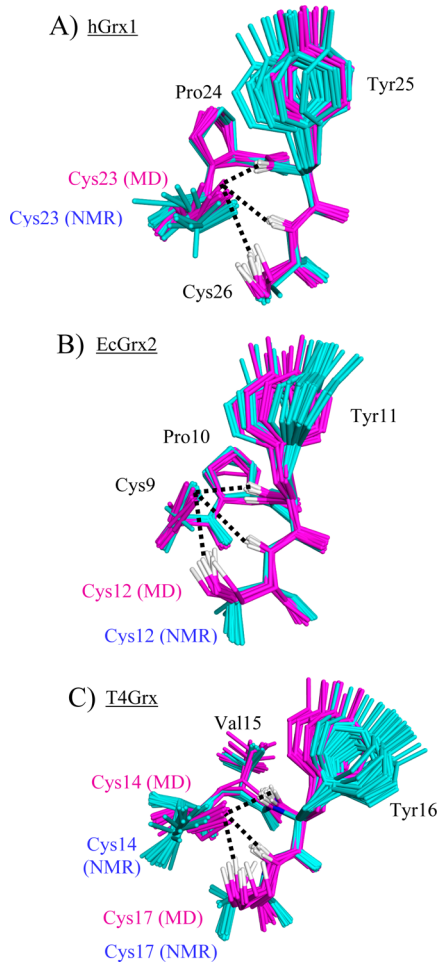

Figure 4. Differences between the structures of the -Cys-X1-X2-Cys- motifs in the MD simulations vs the NMR models. The -Cys-X1-X2-Cys- motifs obtained after MD simulations (magenta with selected white hydrogen atoms) were aligned on their counterpart in the NMR models (light blue, hydrogen atoms not shown for the sake of clarity). The shown hydrogen atoms are in functional groups involved in hydrogen bonds to the thiolate, i.e., in backbone NH groups and the SH groups of the C-ter cysteine. Each panel [(A) hGrx1, (B) EcGrx2, and (C) T4Grx] illustrates the structural reorganization of the -Cys-X1-X2-Cys- motifs after MD simulations, compared to the counterpart NMR conformers. Much of the reorganization consisted of a reorientation of the N-ter or/and the C-ter cysteine side chains. Statistics on the orientation of these side chains are listed in Table 2. During the MD simulations, these side chains changed their orientations such that the thiolate sulfur forms hydrogen bonds (black dotted lines) with the -Cys-X1-X2-Cys- motif. Statistics on these interactions are summarized in Table 3. Overall, in contrast to the NMR conformers, the -Cys-X1-X2-Cys- motif populates a consensus structure in the MD models, allowing the frequent formation of stabilizing hydrogen bonds to the thiolate in the MD snapshots. The consensus MD conformation adopted by the -Cys-X1-X2-Cys- motif in each active site is similar for hGrx1, EcGrx2, and T4Grx. This conformational focusing around the thiolate extends to the tyrosine side chains, which may also stabilize the thiolate via a C−H interaction with hydrogen bond character. Note also the difference in the conformation of Val15 in T4Grx. For the sake of clarity, only MD snapshots taken every 10 ns are shown.

dx.doi.org/10.1021/bi3006576 | *Biochemistry* 2012, 51, 8189−8207

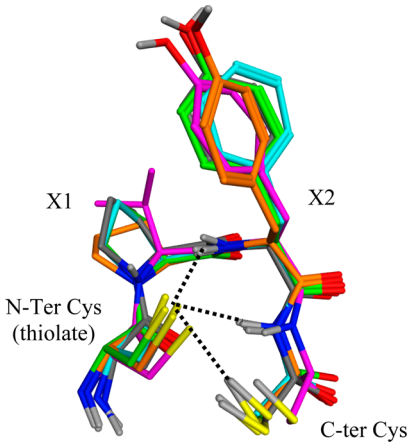

Figure 5. Consensus structure of the -Cys-X1-X2-Cys- active site motif in glutaredoxins. Overlay of representative conformers obtained from MD simulations for reduced hGrx1 (gray carbons), EcGrx2 (orange carbons), T4Grx (magenta carbons), EcGrx3 (green carbons), and pGrx (light blue carbons). The conformers of hGrx1, EcGrx2, and T4Grx were obtained in this work (*hGrx1_a* at 100 ns, *EcGrx2_a* at 100 ns, and *T4Grx_a* at 100 ns) and were selected to be representative of the corresponding active site, with reference to key structural features (Tables 2 and 3). The conformers of EcGrx3 and pGrx were obtained from previous work.[22,25] The consensus structure of the -Cys-X1-X2-Cys- motif corresponds to specific orientations of the cysteine side chains, χ_1 = *trans* for the N-ter cysteine and $\chi_1 = g^-$ for the C-ter cysteine. This structure is functionally relevant because it is essential for the formation of the hydrogen bonds (black dotted lines) stabilizing the thiolate (the sulfur atoms are colored yellow). This work emphasizes the accumulating evidence supporting a common structure for the -Cys-X1-X2-Cys- motif in glutaredoxins; however, there may be departures from this pattern, as illustrated by EcGrx1 (see section The Case of EcGrx1: Departure from the Consensus Structure for the -Cys-X1-X2-Cys- Motif).

formed almost exclusively within the -Cys23-Pro24-Tyr25-Cys26- motif. Virtually no hydrogen bond is formed between the thiolate and Lys20 or Thr22 in the simulations (Table 5), in contrast with the NMR model. These differences are significant because interactions with Lys20 and Thr22 (then called Lys19 and Thr21, respectively[10]) were invoked to interpret the low pK_a of Cys23 (Cys22), although that could not be reconciled with experiment.[10]

Overall, the MD simulations yield a picture of the reduced hGrx1 active site with subtle but significant differences compared to the NMR model. The simulated structures are chemically more accurate because they are consistent with experimental data regarding the functionally important pK_a of the catalytic cysteine. That is despite the great care with which the hGrx1 NMR models were prepared, in particular their refinement with Cys23 as a thiolate.[18] The improvements brought by the MD simulations are not surprising because, in contrast to the NMR models, the protein-simulated conformers are sampled from a proper Boltzmann distribution in explicit solvent. Even more striking differences were observed between MD and NMR models for EcGrx2 and T4Grx (Figure 4), for which the NMR models were refined with a neutral N-ter active site cysteine.

The Structure of the EcGrx2 -Cys9-Pro10-Tyr11-Cys12- Motif Is Not Atypical. EcGrx2 is particularly interesting because its overall fold is atypical for a glutaredoxin.[15,67] This puts the intriguing NMR conformers of the active site -Cys9-Pro10-Tyr11-Cys12- motif (see section Structural Heterogeneity of the NMR Models of the Reduced Active Sites and Calculated pKa Values as a Test of the NMR Models) in a distinctive context. Another particular trait of EcGrx2 is the fact that its His8 is located directly before the -Cys9-Pro10-Tyr11-Cys12- sequence. The protonation state and the potential mechanistic role of this histidine are unknown; to address those issues, a first step is to clarify the local interactions formed by His8, and its conformational dynamics. Thus, His8 was treated as neutral (proton on N^{δ}) in *EcGrx2_a* and *EcGrx2_b* but as protonated (proton on N^{δ} and N^{ϵ}) in *EcGrx2_c*. In the three EcGrx2 simulations (Table1), Cys9 was treated as a thiolate. The starting active site structures for the EcGrx2 simulations are given in Table S1 and Figure S2 of the Supporting Information.

EcGrx2_a and *EcGrx2_c* were initiated with χ_1^{Cys9} in g^+, but χ_1^{Cys9} switched to *trans* in those simulations (Figure 2). Then, χ_1^{Cys9} populated *trans* overwhelmingly in the simulations (Table 2). This orientation of the N-ter cysteine allows the formation of the $S^{\gamma}{}_9\cdots N_{11}$ and $S^{\gamma}{}_9\cdots N_{12}$ hydrogen bonds with the backbone amides (Table 3). Importantly, in *EcGrx2_a*, *EcGrx2_b*, and *EcGrx2_c*, the active site C-ter Cys12 switched to $\chi_1^{Cys12} = g^-$ where it remained most of the time (Figure 3), a difference between the simulated and NMR models (Table 2 and Figure 4B). This reorientation of Cys12 allowed the frequent formation of a thiol−thiolate $S^{\gamma}{}_9\cdots S^{\gamma}{}_{12}$ hydrogen bond (Table 3). A thiol−thiolate hydrogen bond in homologous sites has received direct experimental support.[28,30] We note that the reorientations of Cys9 and Cys12 sometimes required simulation times of at least 20 ns (Figures 2 and 3). The need for simulations well above a few nanoseconds is illustrated again in following sections.

The other active site side chain that showed differences between simulated and NMR models was His8. During the MD simulations, the His8 side chain adopted a more focused conformation [predominantly with χ_1^{His8} in g^+ and χ_2^{His8} in g^-, for both neutral and protonated His8 (Figure S4 of the Supporting Information)] than in the NMR model. In the NMR structure, χ_1^{His8} was mostly *trans*, but this conformer was not stable in the simulations. The simulated conformation of His8 was stabilized by a hydrogen bond between the imidazole ring (donor group, $N^{\delta}{}_8$−H) and the carboxylate of Glu112. Even when protonated, His8 did not form a hydrogen bond to the proximal thiolate of Cys9 (Table 5).

Therefore, with both neutral and protonated His8, the three simulations of EcGrx2 converged toward the same structure for the reduced active site -Cys9-Pro10-Tyr11-Cys12- motif of EcGrx2. This structure is in consensus with those obtained by MD simulations with other glutaredoxin -Cys-X1-X2-Cys- motifs (Figure 5), despite EcGrx2 being an atypical glutaredoxin. Thus, the local structure of the EcGrx2 -Cys9-Pro10-Tyr11-Cys12- motif is not atypical. This stresses that the conservation of this local structure and the associated hydrogen bond pattern are important for the function of this enzyme family, even when the -Cys-X1-X2-Cys- motif is embedded in an atypical architecture.

The similarity between the active site of EcGrx2 and that of other glutaredoxins extends to the calculated pK_a values for the nucleophilic cysteine (Table 4). The pK_a of Cys9 in EcGrx2 was not strongly affected by the protonation state of His8 in the MD, consistent with the lack of a hydrogen bond between the thiolate and His8. The simulated snapshots of EcGrx2 gave an average calculated pK_a of ∼5.4 for Cys9 (Table 4), much closer to the experimentally determined pK_a of ∼3.5 (see section Experimental pKa Determinations for the Cysteines in EcGrx2

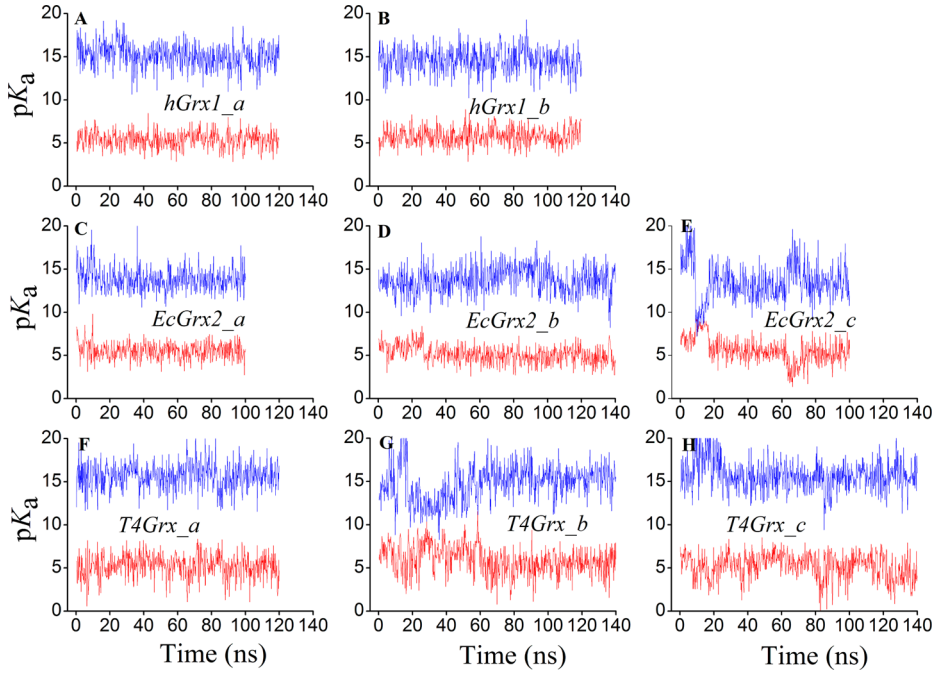

Figure 6. Calculated pK_a values for the active site cysteines along the MD simulations of the glutaredoxins. The calculated pK_a values of the active site N-ter (red) and C-ter (blue) cysteines are plotted vs time during the MD simulations. For each panel, the cysteines and simulation name are as follows: (A) Cys23 and Cys26 in *hGrx1_a*, (B) Cys23 and Cys26 in *hGrx_b*, (C) Cys9 and Cys12 in *EcGrx2_a*, (D) Cys9 and Cys12 in *EcGrx2_b*, (E) Cys9 and Cys12 in *EcGrx2_c*, (F) Cys14 and Cys17 in *T4Grx_a*, (G) Cys14 and Cys17 in *T4Grx_b*, and (H) Cys14 and Cys17 in *T4Grx_c*. The simulation names are defined in Table 1. The pK_a of the N-ter cysteine is consistently much lower than that of the C-ter cysteine. The low pK_a values obtained for the N-ter cysteine strongly support the underlying structural models from MD. The fluctuations in the calculated pK_a values reflect their sensitivity to the structural fluctuations during the simulations.

Table 5. Hydrogen Bonds between the Catalytic Cysteine Sulfur and Side Chains outside the -Cys-X1-X2-Cys- Motif

	acceptor···donor[a]	NMR[b]	MD[c]			
hGrx1		1JHB	*hGrx1_a*	*hGrx1_b*	*hGrx1_K20L*	*hGrx1_K20Q*
	$S^{\gamma}_{23}\cdots N^{\zeta}_{20}$ Lys20	4 (20.0%)	0.5	0.1	NA[d]	NA[d]
	$S^{\gamma}_{23}\cdots O^{\gamma}_{22}$ Thr22	2 (10.0%)	0.0	1.6	0.0	0.3
EcGrx2		1J7O	*EcGrx2_a*	*EcGrx2_b*	*EcGrx2_c*	
	$S^{\gamma}_{9}\cdots N^{\delta}_{8}$ His8	0 (0.0%)	0.0	0.0	0.0	
	$S^{\gamma}_{9}\cdots N^{\epsilon}_{8}$ His8	NA[e]	NA[e]	NA[e]	0.0	
	$S^{\gamma}_{9}\cdots N^{\zeta}_{125}$ Lys125	0 (0.0%)	0.1	0.1	0.0	
T4Grx		1DE2	*T4Grx_a*	*T4Grx_b*	*T4Grx_c*	
	$S^{\gamma}_{14}\cdots N^{\zeta}_{13}$ Lys13	0 (0.0%)	0.0	0.0	0.0	

[a]Possible hydrogen bonds between the sulfur of the N-ter cysteine S^{γ} and potential hydrogen bond donors outside the -Cys-X1-X2-Cys- motif (potential hydrogen bond donor given at the right); the subscripts indicate the residue numbers. [b]Frequency of occurrence of each hydrogen bond in the NMR structures (the PDB entry codes are given), as the number of conformers where the hydrogen bond is observed, and the corresponding percentage relative to the total number of NMR conformers. [c]Frequency of occurrence of each hydrogen bond during the MD simulations (each MD identifier is given), in percent of the time. The geometric criteria used to define the presence of a hydrogen bond are given in Materials and Methods. [d]Not applicable because Lys20 was mutated to Leu or Gln. [e]Not applicable because His8 was modeled as neutral without a protonated N^{ϵ} in NMR structure 1J7O and in simulations *EcGrx2_a* and *EcGrx2_b*.

and T4Grx) than the average pK_a of 8.3 ± 1.3 calculated from the NMR conformers. This is a very strong indication that the structural model yielded by the MD simulations (χ_1^{Cys9} = *trans*, and χ_1^{Cys12} = g^-) is chemically more accurate than its NMR counterpart (Figure 4B).

Conformational Focusing of the T4Grx Active Site via MD Simulations. The sequence of the -Cys14-Val15-Tyr16-Cys17- motif in the active site of T4Grx is somewhat unconventional, because of its valine at position 15, instead of the common proline in glutaredoxins.[2,4] Crystallizing the reduced form of wild-type T4Grx has proven to be challenging;[12] instead, one had to resort to crystallizing the reduced T4Grx mutant -Cys14-Gly15-Pro16-Cys17- motif,[12] which is hardly representative of the wild-type sequence (our understanding is that the resulting X-ray structure is not available from the PDB). On the other hand, the NMR model of the reduced active site of T4Grx[17] is structurally particularly heterogeneous (Figure 1 and Table 2). Thus, three MD simulations with Cys14 as a thiolate were performed for T4Grx (*T4Grx_a*, *T4Grx_b*, and *T4Grx_c*), all starting with different combinations of χ_1^{Cys14} and χ_1^{Cys17} (Table S1 and Figure S3 of the Supporting Information). Each of these simulations converged toward the same structure for the -Cys14-Val15-Tyr16-Cys17- motif (Figure 4C), with χ_1^{Cys14} = *trans* (Figure 2) and χ_1^{Cys17} = g^- (Figure 3). The

dx.doi.org/10.1021/bi3006576 | *Biochemistry* 2012, 51, 8189−8207

structure of the T4Grx -Cys14-Val15-Tyr16-Cys17- motif is in consensus with its counterpart obtained for other glutaredoxins (Figure 5).

The simulated structure of the -Cys14-Val15-Tyr16-Cys17- motif allows the frequent formation of $S^{\gamma}_{14}\cdots N_{16}$, $S^{\gamma}_{14}\cdots N_{17}$, and $S^{\gamma}_{14}\cdots S^{\gamma}_{17}$ hydrogen bonds, which were never formed in the NMR model (Table 3). Thus, the simulations offer a view of the reduced active site of T4Grx very different from that proposed by the NMR model. Crucially, the simulated -Cys14-Val15-Tyr16-Cys17- motif presents essentially the same consensus structure and pattern of hydrogen bonds as with simulated hGrx1 and EcGrx2 (Figure 4C). The presence of the atypical Val15 does not disrupt this consensus arrangement. In the simulations, Val15 adopts predominantly the conformation $\chi_1^{Val15} = g^+$ (Figure S5 of the Supporting Information), while χ_1^{Val15} was in the g^- conformer in all NMR models.

Incidentally, the contact between S^{γ}_{14} and S^{γ}_{17} in the simulations of wild-type T4Grx is reminiscent of the description of the X-ray structure of the reduced -Cys14-Gly15-Pro16-Cys17- sequence in the T4Grx mutant.[12] However, a key difference between the wild type and mutant is that the $S^{\gamma}_{14}\cdots N_{16}$ hydrogen bond cannot be formed with Pro16 in the mutant. On the basis of this observation, we predict that the pK_a of Cys14 in the -Cys14-Gly15-Pro16-Cys17- mutant should be higher than in the wild type.

We note that simulations *T4Grx_b* and *T4Grx_c* took tens of nanoseconds before they converged to the consensus χ_1^{Cys14} = *trans* and $\chi_1^{Cys17} = g^-$ (Figures 2 and 3). For instance, χ_1^{Cys14} in *T4Grx_b* oscillated between *trans* and g^- during the first 60 ns of the simulation (Figure 2); also, χ_1^{Cys17} in *T4Grx_c* oscillated between *trans* and g^- during the first 70 ns of the simulation (Figure 3). This, together with observations from other simulations (e.g., *EcGrx2_b*), shows that simulations of at least tens of nanoseconds may be required to confidently refine NMR models, even for localized conformational changes such as side chain reorganization. One also needs long simulations to probe the conformational dynamics of long flexible side chains around the active site (see section Which Role for the Cationic Side Chains?).

The structural convergence of the three T4Grx simulations is reflected in similar average calculated pK_a values for Cys14 in *T4Grx_a* (pK_a = 5.2 ± 1.3), *T4Grx_b* (pK_a = 5.9 ± 1.6), and *T4Grx_c* (pK_a = 5.2 ± 1.5). These pK_a values calculated along the simulations are clearly lower than the average pK_a of 13.3 ± 2.6 calculated for Cys14 based on the NMR conformers. The large standard deviation for the pK_a of Cys14 with the NMR model reflects the already noted structural heterogeneity of its active site. The average calculated pK_a of Cys14 in the NMR model is much higher than its measured counterpart (Experimental pKa Determinations for the Cysteines in EcGrx2 and T4Grx), in contrast with that derived from the MD snapshots. This is a very strong indication that the conformationally focused structure of the reduced -Cys14-Val15-Tyr16-Cys17- motif of T4Grx4 obtained from MD simulations is chemically more realistic than its disordered counterpart in the NMR model.

An experimental pK_a of 6.8 has been suggested for Cys14 in reduced T4Grx,[17] although without supporting data or experimental details. This is an unusually high pK_a for a glutaredoxin, and it has been proposed that the titration profile of T4Grx is more akin to that of a thioredoxin than that of a glutaredoxin.[17] Even if we assume this unusually high pK_a of 6.8, the MD model and its associated low pK_a would be closer to experiment than the NMR model. Yet, our measured pK_a of 5.1 for Cys14 (see section Experimental pKa Determinations for the Cysteines in EcGrx2 and T4Grx) indicates that the pK_a of the nucleophilic cysteine in T4Grx is not atypical, with a thiolate as stabilized as in other glutaredoxins.[7,9,10]

It has been suggested that a relatively high pK_a of 6.8 for Cys14 in reduced T4Grx (relative to those of other glutaredoxins) results from a paucity of positively charged basic side chains around the T4Grx active site,[17] for instance compared to porcine Grx (pGrx). Yet, a detailed theoretical analysis of the structure, dynamics, and electrostatics of pGrx[25] concluded that the low pK_a (~3.8[7]) of its catalytic Cys22 was not primarily due to long-range electrostatic interactions between Cys22 and surrounding basic residues. Instead, there was every indication that the thiolate of Cys22 is stabilized by direct hydrogen bonds between S^{γ}_{22} and the -Cys22-Pro23-Phe24-Cys25- motif of pGrx. Interpreting the low pK_a of the glutaredoxin N-ter active site cysteine in terms of these hydrogen bonds has a strong explanatory power, contrary to speculation invoking long-range electrostatic interactions. In particular, it explains why mutating basic side chains around reduced glutaredoxin active sites tends to have little impact on the pK_a of their N-ter catalytic cysteine (see section Mutants of hGrx1 Explained).

In the simulations, S^{γ}_{14} in reduced T4Grx is frequently hydrogen-bonded to the -Cys14-Val15-Tyr16-Cys17- motif (Table 3), a feature akin to that proposed to lower the pK_a of the N-ter cysteine in hGrx1 and EcGrx2. Formation of these hydrogen bonds during the simulations explains why the average calculated pK_a of Cys14 is much lower in the simulations than with the NMR model. It is consistent with the average calculated pK_a of Cys14 in *T4Grx_b* being 0.7 pK_a unit higher than in *T4Grx_a* or *T4Grx_c*. Indeed, the hydrogen bonds stabilizing the thiolate are formed less frequently in *T4Grx_b* than in *T4Grx_a* or *T4Grx_c* (Table 3), because during the first 60 ns of *T4Grx_b*, χ_1^{Cys14} and χ_1^{Cys17} populate conformations (g^- and *trans*, respectively) that disrupt these hydrogen bonds. Thus, the average pK_a of Cys14 in *T4Grx_b* is 6.7 ± 1.6 during the first 60 ns of simulation and subsequently drops to 5.4 ± 1.4 (consistent with *T4Grx_a* and *T4Grx_c*).

In summary, the simulations do not support the notion that the active site of T4Grx is unconventional with regard to its structural dynamics. The reduced -Cys14-Val15-Tyr16-Cys17- motif adopts a main consensus conformation in which local hydrogen bonds are again found to be the factor stabilizing its thiolate.

The Case of EcGrx1: Departure from the Consensus Structure for the -Cys-X1-X2-Cys- Motif. A detailed analysis of the structure and dynamics of the -Cys11-Pro12-Tyr13-Cys14- motif of reduced EcGrx1 has already been presented,[22] based on MD simulations directly comparable (same protocols) to those performed here. Each previous EcGrx1 simulation has been extended from 75 to 200 ns (Table 1). These extended simulations confirmed the conclusions from the earlier analysis, with respect to the conformations of the active site cysteines (Table 2) and their hydrogen bonding pattern (Table 3). As with the other glutaredoxins, the C-ter cysteine of EcGrx1 populated overwhelmingly the $\chi_1^{Cys14} = g^-$ conformer. However, the N-ter cysteine of EcGrx1 populated approximately equally the $\chi_1^{Cys11} = g^+$ and χ_1^{Cys11} = *trans* conformers. This contrasts with the overwhelming preference for *trans* of the N-ter cysteine in other glutaredoxins (Table 2). As described before, this greater flexibility of the N-ter cysteine

dx.doi.org/10.1021/bi3006576 | *Biochemistry* 2012, 51, 8189−8207

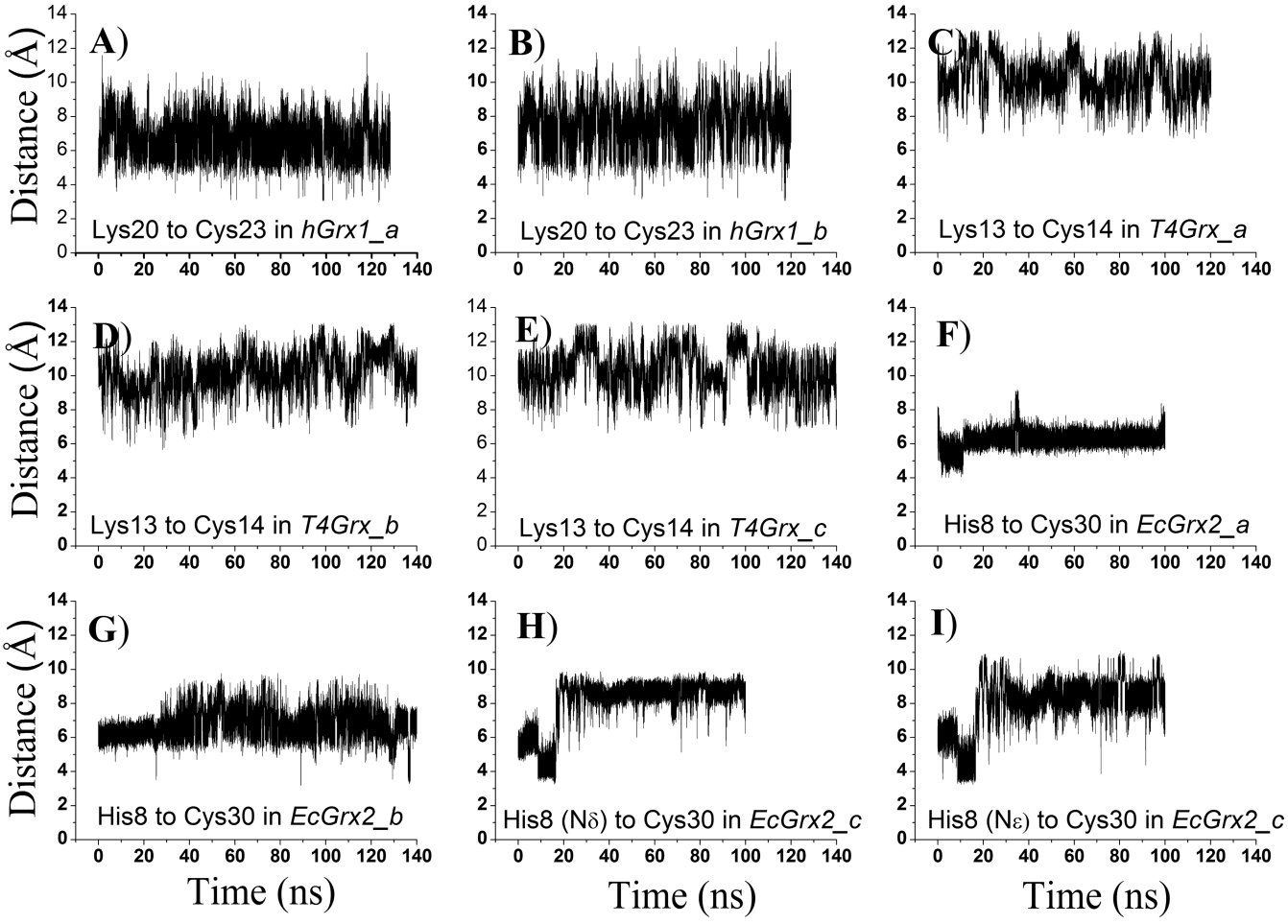

Figure 7. Distances between the thiolate sulfur and selected basic side chains during the MD simulations. The panels show the time course of distances between the thiolate sulfur of the catalytic cysteine and (i) the cationic amino group of Lys20 in hGrx1, (ii) the cationic amino group of Lys13 in T4Grx, and (iii) the $N^{\delta}H/N^{\epsilon}H$ of the His8 indole in EcGrx2. These side chains were selected because they are located shortly upstream from the -Cys-X1-X2-Cys- sequence and could potentially form hydrogen bonds to the thiolate (see the text). The following specific distances are plotted in each panel: (A) $N^{\zeta}{}_{20}$ of Lys20 to $S^{\gamma}{}_{23}$ of Cys23 in *hGrx1_a*, (B) $N^{\zeta}{}_{20}$ of Lys20 to $S^{\gamma}{}_{23}$ of Cys23 in *hGrx1_b*, (C) $N^{\zeta}{}_{13}$ of Lys13 to $S^{\gamma}{}_{14}$ of Cys14 in *T4Grx_a*, (D) $N^{\zeta}{}_{13}$ of Lys13 to $S^{\gamma}{}_{14}$ of Cys14 in *T4Grx_b*, (E) $N^{\zeta}{}_{13}$ of Lys13 to $S^{\gamma}{}_{14}$ of Cys14 in *T4Grx_c*, (F) $N^{\delta}{}_{8}$ of His8 to $S^{\gamma}{}_{9}$ of Cys9 in *EcGrx2_a*, (G) $N^{\delta}{}_{8}$ of His8 to $S^{\gamma}{}_{9}$ of Cys9 in *EcGrx2_b*, (H) $N^{\delta}{}_{8}$ of His8 to $S^{\gamma}{}_{9}$ of Cys9 in *EcGrx2_c*, and (I) $N^{\epsilon}{}_{8}$ of His8 to $S^{\gamma}{}_{9}$ of Cys9 in *EcGrx2_c*. The $N^{\epsilon}{}_{8}$–$S^{\gamma}{}_{9}$ distance is plotted for *EcGrx2_c* because His8 was protonated in this simulation, but not in *EcGrx2_a* and *EcGrx2_b*. Hydrogen bonds between the thiolate and the selected groups would correspond to short distances (≤4 Å), which occurs only rarely.

in EcGrx1 reflects the intermittent hydrogen bonding of its thiolate by Arg8.[22] EcGrx1 is so far the only glutaredoxin for which a frequent direct hydrogen bond between the thiolate and a peripheral cationic side chain has been observed.

Thus, the EcGrx1 -Cys11-Pro12-Tyr13-Cys14- sequence adopts most features of the consensus structure of the -Cys-X1-X2-Cys- motif observed in other glutaredoxins. The frequent population of $\chi_1{}^{Cys11} = g^+$ for the N-ter cysteine of EcGrx1 is the main departure from the consensus structure. It is still compatible with a low pK_a of Cys11 in EcGrx1, because of the hydrogen bond between the thiolate and Arg8.[22] Incidentally, the greater flexibility of the N-ter cysteine in simulations of EcGrx1 stresses the fact that the ordered conformations of the cysteines in the simulated -Cys-X1-X2-Cys- motifs do not result from imbalances in the force field, as demonstrated previously.[25] The departure of the -Cys11-Pro12-Tyr13-Cys14- motif from the consensus conformation in EcGrx1 appears to be an exception because the consensus structure has been observed for EcGrx3,[22] pig glutaredoxin,[25] hGrx1, EcGrx2, and T4Grx.

Which Role for the Cationic Side Chains? It has frequently been assumed that the low pK_a of the N-ter active site cysteine in enzymes of the Trx superfamily reflects the influence of peripheral cationic (basic) residues.[3,7,10,17,29,30] This, however, fails to explain how such long-range electrostatic effects could specifically impart a low pK_a to the N-ter Cys, while allowing a much higher pK_a for its neighboring C-ter Cys. Also, such a mechanism would put particular functional constraints on the conservation of the peripheral charged side chains. However, there is no clear conservation of the basic side chains around the glutaredoxin active sites,[4,17] which may have evolved to recognize diverse substrates rather than maintain the pK_a of the catalytic cysteine. Therefore, the conformational dynamics of the side chains around the active site is also of interest with regard to glutaredoxin substrate recognition.

This work generalizes the initial suggestion[9] that the pK_a of the N-ter cysteine is primarily controlled by direct hydrogen bonds between the -Cys-X1-X2-Cys- motif and the thiolate. However, basic and flexible side chains peripheral to the -Cys-X1-X2-Cys- motif could conceivably reach and form a hydrogen

dx.doi.org/10.1021/bi3006576 | *Biochemistry* 2012, 51, 8189–8207

bond with the thiolate. This is particularly pertinent for lysines or arginines located in the N-terminal proximity of the -Cys-X1-X2-Cys- sequence,[22,75] which may approach the solvent-accessible face of the thiolate, even when the thiolate is chelated to the -Cys-X1-X2-Cys- motif. Candidate side chains (N-terminal of the -Cys-X1-X2-Cys- motif) include Lys20 in hGrx1 and Lys13 in T4Grx. It has already been explained above that His8 in EcGrx2 did not form a hydrogen bond with the thiolate. The frequency of hydrogen bonds between the thiolate and selected side chains outside the -Cys-X1-X2-Cys- motif is summarized in Table 5.

Mutants of hGrx1 Explained. In the NMR structure of hGrx1, Lys20 forms a hydrogen bond with the thiolate in four conformers. This could suggest that Lys20 is the likely molecular basis for the low pK_a of Cys23[10] (the hGrx1 residue numbering in ref 10 is offset by 1 relative to that used here, such that Lys20 and Cys23 are called Lys19 and Cys22, respectively). Thus, mutants Lys20Leu and Lys20Gln were produced experimentally, and the pK_a of their Cys23 was measured,[10] using the pH dependence of the inactivation of the enzyme by iodoacetamide. The Lys20Leu and Lys20Gln mutants were obtained in two constructs:[10] (i) the "single-cysteine" construct SC-Grx in which only Cys23 was kept and Cys26 was mutated to serine and (ii) the "triple-mutant" construct TM-Grx in which both Cys23 and Cys26 were retained. SC-Grx gave the following experimental pK_a values for Cys23: 4.2 ± 0.09 with Lys20, 4.6 ± 0.05 for Lys20Leu, and 5.0 ± 0.11 for Lys20Gln.[10] TM-Grx gave the following experimental pK_a values for Cys23: 3.6 ± 0.06 with Lys20, 3.7 ± 0.09 for Lys20Leu, and 3.7 ± 0.08 for Lys20Gln.[10] The important point is that, with both SC-Grx and TM-Grx, the pK_a of Cys23 was barely perturbed by the mutation of Lys20 to Leu or Gln. These results were at variance with the molecular modeling predictions presented in the same study,[10] which had suggested that the low pK_a of Cys23 would result primarily from an ion pair between the thiolate and the positively charged Lys20. Hence, the study[10] provided very useful experimental data but struggled in their interpretation to elucidate the molecular basis of the low pK_a of Cys23. Here, we revisit this question and show that the protein dynamics emerging from the MD simulations is necessary to understand the experimental data.

We simulated the Lys20Leu and Lys20Gln mutants of hGrx1, each for 60 ns. The average calculated pK_a of Cys23 along these simulations was 5.4 ± 0.9 (Lys20Leu) or 5.7 ± 0.9 (Lys20Gln), compared to 5.6 ± 0.9 for the wild type (merged data from *hGrx1_a* and *hGrx1_b*). Thus, our protocol yields a Cys23 pK_a as low in the mutants as in the wild type, consonant with experiment.[10] Our theoretical investigation also concludes that Lys20 is not a major determinant of the low pK_a of Cys23 in hGrx1. This can be understood by examining the distance between the amino group of Lys20 and the thiolate during the MD simulations (Figure 7A,B). This distance fluctuated dynamically around averages of 6.6 Å (*hGrx1_a*) and 7.4 Å (*hGrx1_b*). In the simulations, a hydrogen bond between the amino group of Lys20 and the thiolate is rarely formed, 0.5% (*hGrx1_a*) and 0.1% (*hGrx1_b*) of the time. Instead, the Lys20 side chain is most of the time pointing away from the thiolate, with the electrostatic interactions between these two groups being screened by hydration. Therefore, the NMR model of hGrx1 over-represented the ionic pair between Lys20 and the thiolate, which led to the assignment of too much weight to this interaction in previous analyses.[10] This shows that obtaining thermodynamically relevant populations for the conformers is critical; that can hardly be achieved without simulations in explicit solvent at the temperature of interest. It illustrates how MD simulations offer much-needed insights regarding the structure and dynamics of long flexible side chains at a protein surface, another critical aspect of the refinement of NMR models.

Like the wild type, the simulated Lys20Leu and Lys20Gln hGrx1 mutants formed the three key hydrogen bonds ($S^{\gamma}_{23}\cdots N_{25}$, $S^{\gamma}_{23}\cdots N_{26}$, and $S^{\gamma}_{23}\cdots S^{\gamma}_{26}$) between the thiolate and the -Cys23-Pro24-Tyr25-Cys26- motif (Table 3). As in the wild type, these hydrogen bonds are sufficient to rationalize the low pK_a of Cys23 in the mutants. Although it was reasonable to invoke a hydrogen bond between the thiolate and Thr22,[10] such an interaction is virtually never formed in the hGrx1 mutants or in the wild type (Table 5). The low pK_a of Cys23 can be explained without invoking such interaction. Indeed, Thr22 is not conserved in glutaredoxins.[10] Overall, this computational analysis rationalizes the pK_a measurements obtained for the hGrx1 Lys20Leu and Lys20Gln mutants. This further strengthens our emphasis of local hydrogen bonds between the thiolate and the -Cys-X1-X2-Cys- motif to explain the low pK_a of the catalytic cysteine.

The benefits of MD simulations are clear upon comparison of this investigation to one that could use only the NMR conformers as a structural basis.[10] When relying solely on the NMR conformers, an otherwise sound analysis could not discern the factors stabilizing the thiolate, because the underlying structures were too crude. The chemical relevance of the reduced hGrx1 structure was dramatically improved when using an ensemble simulated for tens of nanoseconds in explicit solvent.

Simulations Propose an Alternative Recognition Surface for Reduced T4Grx and EcGrx2. The thiol-disulfide oxidoreductases act preferentially on some substrates,[1,5,76] implying elements of specific recognition between a particular oxidoreductase and its substrates. The mechanisms mediating the recognition between thiol-disulfide oxidoreductase and substrate remain largely unknown, although important glimpses have been captured.[45,76−78] For instance, a structural analysis of a mixed disulfide between EcGrx1 and a peptide mimic of its ribonucleotide reductase substrate emphasized the importance of electrostatic interactions to rationalize the specificity of the interaction between EcGrx1 and ribonucleotide reductase.[76] Thus, the specific substrate recognition by glutaredoxins is expected to actively involve the side chains surrounding the -Cys-X1-X2-Cys- motif. Hence, we examined the conformational spread and dynamics of some of these side chains. In that respect, the behavior of long flexible charged side chains is particularly intriguing, for instance, if one contemplated computational docking experiments between reduced glutaredoxins and their substrates. A detailed study of these issues is beyond the scope of this work; however, their relevance can be illustrated with particular examples.

Figure 8A shows the conformational spread of Lys13 and Asp18 of reduced T4Grx, in simulation *T4Grx_a* compared to the NMR model (simulations *T4Grx_b* and *T4Grx_c* yielded results similar to those of simulation *T4Grx_a*). Lys13 and Asp18 are adjacent in sequence to the -Cys14-Val15-Tyr16-Cys17- motif. Figure 8A shows that the region of space occupied by Lys13 and Asp18 differs between the simulated and NMR models. The difference regarding Lys13 is striking, as it points in a very different direction after the NMR model was

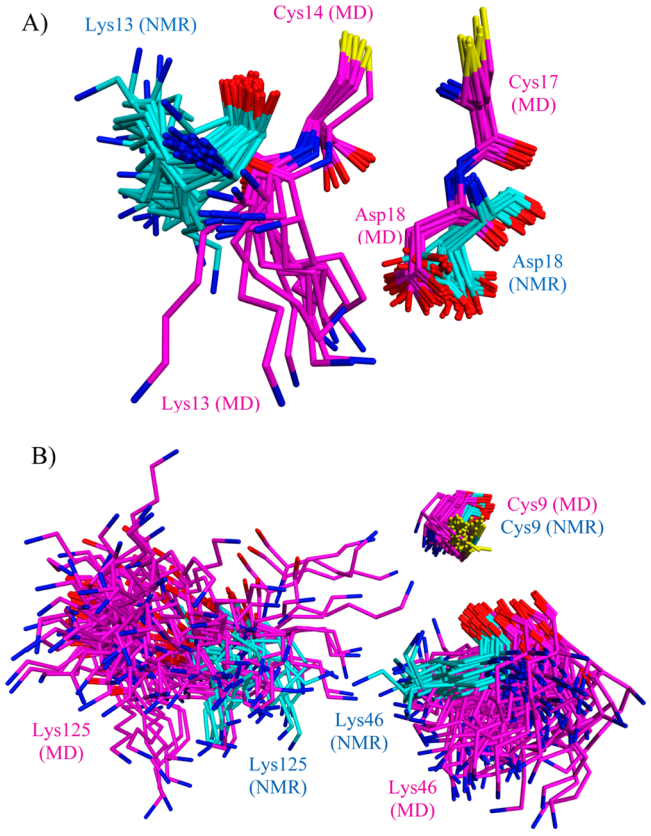

Figure 8. Comparison of simulated vs NMR models around the reduced active sites. Snapshots extracted from MD simulations (magenta carbons) were overlaid on the corresponding NMR model (blue carbons) for T4Grx (A) and EcGrx2 (B). For the sake of clarity, only selected residues are shown. (A) MD snapshots are from *T4Grx_a*, with emphasis on Lys13 and Asp18, which are adjascent in sequence to the -Cys14-Val15-Tyr16-Cys17- active site motif of T4Grx. In the simulation, Lys13 occupies a very different area of space as compared to that in the NMR model. The simulated Lys13 intermitently forms a salt bridge with Asp18, not observed in the NMR model. (B) MD snapshots are from *EcGrx2_a*, with emphasis on Lys46 and Lys125, which are in the vicinity of the active site in the tertiary structure. In the simulation, Lys46 and Lys125 cover a broader conformational space than in the NMR model. Overall, the MD simulations suggest a new molecular shape and electrostatic character around the reduced active sites of T4Grx and EcGrx2, as compared to the NMR models. The implications for substrate recognition are discussed in the text.

subjected to MD simulation in explicit solvent. During the simulation, the Lys13 side chain was fully reoriented to form an intermittent salt bridge with Asp18 (Figure 8A). Consequently, the average location of the Asp18 side chain also differs after simulation of the NMR model. Differences between the simulated and NMR model are also illustrated with EcGrx2 in Figure 8B, where the conformational spread of Lys46 and Lys125 is greater after MD simulation.

The reorganization of charged side chains at the periphery of the active site usually has an only marginal impact on the pK_a of the catalytic cysteine, as shown explicitly above with hGrx1. However, such adjustments remain an important outcome of the refinement of the NMR models by MD simulations, because they provide a different structural basis for further analyses, e.g., pertaining to substrate recognition and electrostatic interactions. Therefore, our work proposes that reduced T4Grx and EcGrx2 present to their substrates recognition molecular surfaces around their active sites that differ significantly from those in the NMR structures.

Experimental pK_a Determinations for the Cysteines in EcGrx2 and T4Grx. Figure 9A shows the experimental titration of the two cysteines of EcGrx2 from pH 2.7 to 10. Wild-type EcGrx2 has two thiols at its active site, expected to have different pK_a values. Three areas can be observed in the titration curve: between pH 2.7 and 5, between pH 5 and 8, and at pH >8. Between pH 5 and 8, there was no significant change in absorbance, showing no change in the total concentration of thiolates. The inflection point of sigmoidal models fitted to the titration points at pH ≤7.5 was at pH 3.5. Considering that this titration was incomplete at the lowest extreme of pH, the value of 3.5 is interpreted as a higher bound of the corresponding pK_a. Thus, the area below pH 5 corresponds to a decrease in the thiolate concentration and most likely represents the titration of a thiolate with an apparent pK_a of ∼3.5 or less. The area above pH 8 shows an increase in thiolate concentration. The corresponding thiol must have a very high apparent pK_a (≥9.5). These data suggest the titration of two thiol groups for EcGrx2, one with a pK_a of ≤3.5 and another with a pK_a of >9.5. Given the described mechanism for the reduction of target

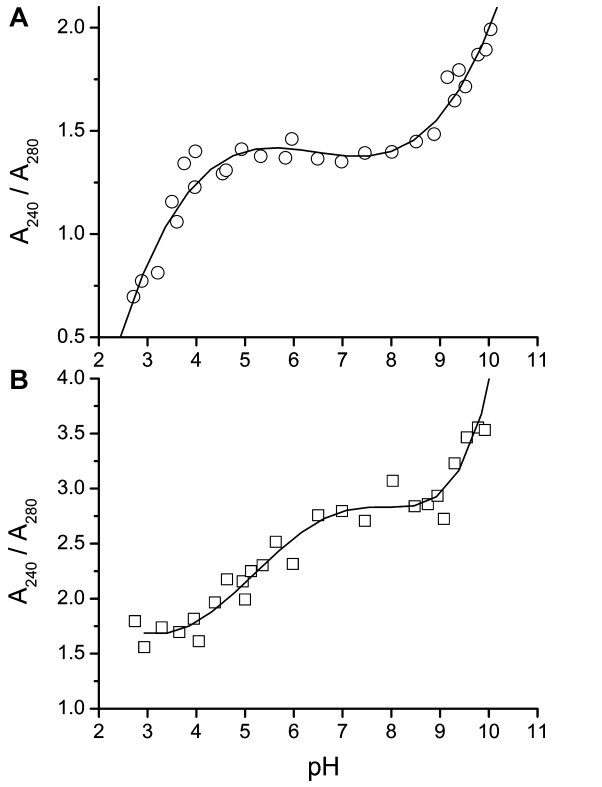

Figure 9. Experimental pH titrations of the cysteines of EcGrx2 and T4Grx. The titration curves of EcGrx2 [(A) ○] and T4Grx [(B) □] are shown vs pH. The presence of thiolate was monitored spectroscopically by the ratio A_{240}/A_{280}, where A_{240} is the absorbance of the thiolate anion at 240 nm and A_{280} is the protein absorbance at 280 nm. The solid black curves were obtained by fitting a polynomial function to the experimental data, to emphasize the overall shape of the titration curves. Each curve revealed the titration of two thiols, at low pH (<7) and at high pH (>7). The titrations at high pH were not complete for either EcGrx2 or T4Grx. The titration of EcGrx2 at low pH was also incomplete, although a more complete titration was obtained at low pH for T4Grx. Note the different scales on the *y*-axes.

dx.doi.org/10.1021/bi3006576 | *Biochemistry* 2012, 51, 8189−8207

disulfides by the members of the thioredoxin/glutaredoxin superfamily,[1,6] the low-pK_a thiolate most likely corresponds to the attacking cysteine (Cys9) while the high-pK_a thiolate represents the resolving cysteine (Cys12).

Another experimental curve containing two titration regions was obtained for T4Grx (Figure 9B), consistent with T4Grx containing two cysteines. The inflection point of the fitted sigmoidal model gave an estimated pK_a of 5.1 for the cysteine titrating at low pH, while the cysteine titrating at high pH had a pK_a of >9.5. The low pK_a of ∼5.1 is lower than the value of 6.8 previously mentioned.[17] Different measured values for the pK_a of the attacking cysteine thiolate of *E. coli* thioredoxin are not unprecedented,[28,79] and artificially high measured pK_a values may be attributed to the oxidation of the low-pK_a thiolate species during measurements, lowering its apparent concentration. These titration curves appear to be reliable, considering the relatively large amounts of glutaredoxins used, the direct spectroscopic measurement of the thiolate concentration, and the concurrent monitoring of the oxidation state of thiols. It was proposed[17] that, with a cysteine pK_a of 6.8, T4Grx would have a chemistry more akin to that of a thioredoxin than that of a glutaredoxin; our measurements, however, do not support this notion.

The molecular simulations and electrostatic analyses of EcGrx2 (The Structure of the EcGrx2 -Cys9-Pro10-Tyr11-Cys12- Motif Is Not Atypical) and T4Grx (Conformational Focusing of the T4Grx Active Site via MD Simulations) allow the confident assignment of their cysteines with low and high pK_a values. In EcGrx2, the low-pK_a thiolate is assigned to Cys9 and the high-pK_a thiol to Cys12. In T4Grx, the low-pK_a thiolate is assigned to Cys14 and the high-pK_a thiol to Cys17. These assignments are consistent with the expectation that it is the N-ter cysteine in the -Cys-X1-X2-Cys- motif that is nucleophilic, with a low pK_a. However, the significance of the experimental results goes beyond the assignment of low- and high-pK_a thiols to the active site cysteines. Indeed, in combination with the computational studies described above, the pK_a measurements contribute some structural information. Importantly, by confirming the presence of a low-pK_a cysteine, the pK_a measurements support the structural models that are consistent with stabilization of a thiolate. Therefore, the low measured pK_a values assigned to Cys9 (EcGrx2) and Cys13 (T4Grx) are a very strong validation of the structural models obtained by MD simulations for the active sites of EcGrx2 and T4Grx.

CONCLUSIONS

Obtaining X-ray structures of the reduced form of thiol-disulfide oxidoreductases has proven to be challenging.[12,13] Therefore, NMR has been the experimental technique of choice for characterizing structurally the reduced form of these enzymes.[14,15,17,18,80] Importantly, NMR can reveal the overall fold and architecture for these proteins. Also, NMR techniques can provide invaluable pK_a measurements.[9,28] However, the NMR models provided a heterogeneous and inconsistent structural picture of the reduced active sites of glutaredoxins, in particular regarding the conformations of the conserved catalytic -Cys-X1-X2-Cys- motifs. Because a perceived advantage of NMR is that it can probe the conformation and dynamics of biomolecules in solution, there was a possibility that the differences in the NMR models of the -Cys-X1-X2-Cys- motifs reflected true differences. Such differences could have arisen from atypical -Cys-X1-X2-Cys- glutaredoxin sequences such as in T4Grx, or from the -Cys-X1-X2-Cys-motif being embedded in an atypical overall architecture as in EcGrx2. On the other hand, there was the concern that conformational inconsistencies in the reduced NMR-generated -Cys-X1-X2-Cys- motifs could be artifactual, maybe because of a lack of NMR restraints or limitations in the refinement of the NMR models. The aim of this work was to resolve these uncertainties by subjecting relevant NMR models of diverse reduced -Cys-X1-X2-Cys- motifs to extensive MD simulations in explicit solvent, pK_a calculations, and experimental testing. Key to this strategy is the ability of MD simulation to include the influence of explicit solvent and to yield in principle a thermodynamically relevant ensemble of protein conformers, given sufficient sampling. Thus, this work illustrates the complementarity between the NMR and MD simulation approaches for structural determination.

These results clarify the structural features underpinning the low pK_a of the reactive Cys and provide a basis for future studies of reduced hGrx1, EcGrx2, and T4Grx. Glutaredoxins hGrx1, EcGrx2, and T4Grx were selected for this investigation because their active sites offer distinct sequence and architectural variations, and the NMR models of their reduced -Cys-X1-X2-Cys- motifs exhibited striking differences. Upon MD simulations, the -Cys-X1-X2-Cys- motifs in these three enzymes underwent conformational changes, and all converged toward a largely predominant consensus conformation (Figure 5) in which the N-ter and C-ter cysteines adopt χ_1 = *trans* and $\chi_1 = g^-$, respectively. In this consensus conformation, the thiolate of the N-ter cysteine is stabilized by three hydrogen bonds, with (i) the backbone NH group of X2, (ii) the backbone NH group of the C-ter cysteine, and (iii) the thiol SH group of the C-ter cysteine (consistent with direct experimental observations with homologous systems[28,30]). This consensus conformation is the same as that observed before for reduced *E. coli* Grx3[9] and reduced pig glutaredoxin.[25] There is every indication that convergence to this consensus conformation does not result from a bias in the force field used during the MD simulations,[25] as confirmed by our simulations of EcGrx1. Therefore, we conclude that the consensus conformation of the reduced glutaredoxin motif obtained in our MD simulations is representative of the reduced active site of most glutaredoxins. Considering homologies of sequence and function, we suspect that the structural organization of the -Cys-X1-X2-Cys- motif emerging with these systems is likely to be able to be transferred to many other glutaredoxins. Of course, this strategy can be extended to any member of the Trx superfamily for which MD simulations can be performed in combination with pK_a calculations. Coupling this approach with targeted experiments should ultimately provide improving insights into the factors modulating the electrostatics and redox potentials across the Trx superfamily.

The consensus structure of the reduced -Cys-X1-X2-Cys- motif is strongly supported by the accompanying pK_a calculations and experimental measurements. Structural models of the reduced glutaredoxin active sites must account for the typically low pK_a of their catalytic cysteine. By and large, the NMR models did not account for this low pK_a (although the NMR structure of hGrx1 was more realistic than others). In contrast, the consensus structural model of the -Cys-X1-X2-Cys- motif proposed after MD simulations for hGrx1, EcGrx2, and T4Grx (Figure 5) does account for the large decrease in the pK_a of its N-ter cysteine, as examined with Poisson–Boltzmann-based pK_a calculations. This lowered pK_a simply results from hydrogen bonds stabilizing the thiolate in the

dx.doi.org/10.1021/bi3006576 | *Biochemistry* 2012, 51, 8189–8207

consensus conformation of the -Cys-X1-X2-Cys- motif, consistent with homologous systems.[9,73] Therefore, the MD models offer a chemically relevant and intuitively interpretable view of the reduced active sites of hGrx1, EcGrx2, and T4Grx.

Using pK_a calculations to test, validate, and select chemically relevant protein conformers is a somewhat new procedure in structural biochemistry.[22,41] This approach has been proposed to select plausible conformers from an NMR structure.[41] However, with EcGrx2 and T4Grx, none of the NMR conformers yielded satisfactory calculated pK_a values (Tables S3 and S4 of the Supporting Information). This stresses that a pK_a-based selection strategy is most promising when used in combination with simulations that can exploit the NMR conformers as a starting point for further structural refinement. This work shows that MD simulations of tens of nanoseconds may be required for such structural refinement, even when it involves only a few critical side chains.

In addition, MD simulations provide in principle physically sound conformational ensembles for the residues surrounding the active site. Our analysis of reduced hGrx1, EcGrx2, and T4Grx strengthened and extended the previous proposal[9,22] that the basic side chains around the active site are not required to stabilize the catalytic thiolate. Indeed, our calculations on the Lys20Leu and Lys20Gln hGrx1 mutants found that the pK_a of their nucleophilic cysteine is essentially as low as in wild-type hGrx1, consistent with the experimental data.[10] That is because the electrostatic interactions between the thiolate and the Lys20 amino functionality are screened by water, because these two groups are very rarely in direct contact. We also find that the thiolate of Cys23 in hGrx1 is not hydrogen-bonded by Thr22. In the same vein, we did not observe hydrogen bonds between His8 and the thiolate of Cys9 in simulated EcGrx2. Our calculations suggest that His8 is neutral in reduced EcGrx2, and we propose that this be tested experimentally. Our computations predicted that the same principles would hold for reduced T4Grx. The calculated pK_a for the nucleophilic Cys14 of T4Grx was predicted to be essentially as low as with other reduced glutaredoxins. This has been confirmed experimentally here, with a measured pK_a of 5.1 for Cys14 of reduced T4Grx, lower than the value previously suggested.[17] Thus, a different distribution of basic side chains around the T4Grx active site, compared to, e.g., pig glutaredoxin,[17] has little impact on the pK_a of its nucleophilic cysteine. This confirms that the glutaredoxin -Cys-X1-X2-Cys- motif is usually self-contained with regard to the stabilization of its catalytic thiolate via local hydrogen bonds. Thus, the -Cys-X1-X2-Cys- motif functions with the same principles when embedded in an atypical fold as in EcGrx2.

We note that departures from the consensus conformation for the -Cys-X1-X2-Cys- glutaredoxin motif described above are likely to exist, as illustrated with EcGrx1. Such departures may be of special interest in understanding and dissecting the factors modulating the properties and functions of the glutaredoxins.

Overall, MD simulations combined with pK_a calculations are powerful tools for exploring and interpreting the reduced active sites of oxidoreductases of the Trx superfamily. However, the pK_a calculations are only semiquantitative because they depend on a number of operational parameters, notably the protein dielectric constant. Thus, even assuming adequate structures, uncertainties remain with regard to the accuracy of the calculated pK_a values. Therefore, it remains important to measure experimentally the pK_a of the nucleophilic active site cysteine. Here, the measured pK_a value for EcGrx2 was $\leq$3.5.

Using MD simulations to probe the conformational dynamics of the thiol-disulfide oxidoreductases will also provide a stronger basis for understanding the molecular recognition of their substrates. That is because simulations in explicit solvent can provide a different, and more accurate, view of the molecular recognition surface around the enzyme active sites. Improved or new information about the structure and dynamics at the protein surface is of special interest, because much of the protein function depends on the nature of its surface, for recognition and contact with substrates. This was vividly illustrated here with residues around the T4Grx (e.g., Lys13 and Asp18) and EcGrx2 (Lys46 and Lys125) active site. This paves the way for future studies to relate the MD conformational ensembles of the reduced glutaredoxins to the selective recognition of their glutathionylated substrates.

■ ASSOCIATED CONTENT

Supporting Information

A list of structural descriptors for the reduced cysteines before they were subjected to MD simulations (Table S1), calculated pK_a values for Cys23 and Cys26 in the NMR structure of reduced hGrx1 (Table S2), calculated pK_a values for Cys9 and Cys12 in the NMR structure of reduced EcGrx2 (Table S3), calculated pK_a values for Cys14 and Cys17 in the NMR structure of reduced T4Grx (Table S4), starting NMR conformers for the MD simulations of EcGrx1 (Figure S1), starting NMR conformers for the MD simulations of EcGrx2 (Figure S2), starting NMR conformers for the MD simulations of T4Grx (Figure S3), the conformation of the His8 side chain during the simulations of EcGrx2 (Figure S4), and the conformation of the Val15 side chain during the simulations of T4Grx (Figure S5). This material is available free of charge via the Internet at http://pubs.acs.org.

■ AUTHOR INFORMATION

Corresponding Author

*N.F.: e-mail, nf_research@hotmail.com; phone, (+44) (0) 1223 895 338. L.N.: e-mail, lennart.nilsson@ki.se; phone, (+46) (0) 8-524 81099.

Funding

This work was supported by the Swedish Research Council.

Notes

The authors declare no competing financial interest.

■ ABBREVIATIONS

3D, three-dimensional; ABNR, adopted-basis Newton−Raphson; EcGrx1, *E. coli* glutaredoxin 1; EcGrx2, *E. coli* glutaredoxin 2; EcGrx3, *E. coli* glutaredoxin 3; hGrx1, human glutaredoxin 1; MD, molecular dynamics; NMR, nuclear magnetic resonance; PB, Poisson−Boltzmann; PDB, Protein Data Bank; pGrx, pig glutaredoxin; rmsd, root-mean-square deviation; SD, standard deviation; T4Grx, glutaredoxin from virus T4; Trx, thioredoxin; ε_P, protein dielectric constant.

■ REFERENCES

(1) Gallogly, M. M., Starke, D. W., and Mieyal, J. J. (2009) Mechanistic and Kinetic Details of Catalysis of Thiol-Disulfide Exchange by Glutaredoxins and Potential Mechanisms of Regulation. *Antioxid. Redox Signaling 11*, 1059−1081.

(2) Holmgren, A. (1989) Thioredoxin and Glutaredoxin. *J. Biol. Chem. 264*, 13963−13966.

(3) Carvalho, A. P., Fernandes, P. A., and Ramos, M. J. (2006) Similarities and differences in the thioredoxin superfamilly. *Prog. Biophys. Mol. Biol. 91*, 229−248.
(4) Sagemark, J., Elgan, T. H., Burglin, T. R., Johansson, C., Holmgren, A., and Berndt, K. D. (2007) Redox properties and evolution of human glutaredoxins. *Proteins 68*, 879−892.
(5) Gravina, S. A., and Mieyal, J. J. (1993) Thioltransferase is a Specific Glutathionyl Mixed Disulfide Oxidoreductase. *Biochemistry 32*, 3368−3376.
(6) Vlamis-Gardikas, A. (2008) The multiple functions of the thiol-based electron flow pathways of *Escherichia coli*: Eternal concepts revisited. *Biochim. Biophys. Acta 1780*, 1170−1200.
(7) Yang, Y., and Wells, W. W. (1991) Identification and Characterization of the Functional Amino Acids at the Active Center of Pig Liver Thioltransferase by Site-directed Mutagenesis. *J. Biol. Chem. 266*, 12759−12765.
(8) Mieyal, J. J., Starke, D. W., Gravina, S. A., and Hocevar, B. A. (1991) Thioltransferase in Human Red Blood Cells: Kinetics and Equilibrium. *Biochemistry 30*, 8883−8891.
(9) Foloppe, N., Sagemark, J., Nordstrand, K., Berndt, K. D., and Nilsson, L. (2001) Structure, Dynamics and Electrostatics of the Active Site of Glutaredoxin 3 from *Escherichia coli*: Comparison with Functionally Related Proteins. *J. Mol. Biol. 310*, 449−470.
(10) Jao, S.-C., English Ospina, S. M., Berdis, A. J., Starke, D. W., Beth Post, C., and Mieyal, J. J. (2006) Computational and Mutational Analysis of Human Glutaredoxin (Thioltransferase): Probing the Molecular Basis of the Low pK_a of Cysteine 22 and Its Role in Catalysis. *Biochemistry 45*, 4785−4796.
(11) Martin, J. L. (1995) Thioredoxin: A fold for all reasons. *Structure 3*, 245−250.
(12) Ingelman, M., Nordlund, P., and Eklund, H. (1995) The structure of a reduced mutant T4 glutaredoxin. *FEBS Lett. 370*, 209−211.
(13) Bacik, J.-P., and Hazes, B. (2007) Crystal Structures of a Poxviral Glutaredoxin in the Oxidized and Reduced States Show Redox-correlated Structural Changes. *J. Mol. Biol. 365*, 1545−1558.
(14) Sodano, P., Xia, T., Bushweller, J. H., Björnberg, O., Holmgren, A., Billeter, M., and Wüthrich, K. (1991) Sequence-specific ^{1}H NMR Assignments and Determination of the Three-dimensional Structure of Reduced *Escherichia coli* Glutaredoxin. *J. Mol. Biol. 221*, 1311−1324.
(15) Xia, B., Vlamis-Gardikas, A., Holmgren, A., Wüthrich, K., Wright, P. E., and Dyson, H. J. (2001) Solution Structure of *Escherichia coli* glutaredoxin-2 Shows Similarity to Mammalian Glutathione-S-transferases. *J. Mol. Biol. 310*, 907−918.
(16) Fladvad, M., Bellanda, M., Fernandes, A. P., Mammi, S., Vlamis-Gardikas, A., Holmgren, A., and Sunnerhagen, M. (2005) Molecular Mapping of Functionalities in the Solution Structure of Reduced Grx4, a Monothiol Glutaredoxin from *Escherichia coli*. *J. Biol. Chem. 280*, 24553−24561.
(17) Wang, Y., Amegbey, G., and Wishart, D. S. (2004) Solution structures of reduced and oxidized bacteriophage T4 glutaredoxin. *J. Biomol. NMR 29*, 85−90.
(18) Sun, C., Berardi, M. J., and Bushweller, J. H. (1998) The NMR Solution Structure of Human Glutaredoxin in the Fully Reduced Form. *J. Mol. Biol. 280*, 687−701.
(19) Wuthrich, K. (1990) Protein Structure Determination in Solution by NMR Spectroscopy. *J. Biol. Chem. 265*, 22059−22062.
(20) Guntert, P. (1998) Structure calculations of biological macromolecules from NMR data. *Q. Rev. Biophys. 31*, 145−237.
(21) Billeter, M., Wagner, G., and Wuthrich, K. (2008) Solution NMR structure determination of proteins revisited. *J. Biomol. NMR 42*, 155−158.
(22) Foloppe, N., and Nilsson, L. (2004) The glutaredoxin -C-P-Y-C- motif: Influence of peripheral residues. *Structure 12*, 289−300.
(23) Grauschopf, U., Winther, J. R., Korber, P., Zander, T., Dallinger, P., and Bardwell, J. C. A. (1995) Why is DsbA Such an Oxidizing Disulfide Catalyst? *Cell 83*, 947−955.
(24) Huber-Wunderlich, M., and Glockshuber, R. (1998) A single dipeptide sequence modulates the redox properties of a whole enzyme family. *Folding Des. 3*, 161−171.
(25) Foloppe, N., and Nilsson, L. (2007) Stabilization of the Catalytic Thiolate in a Mammalian Glutaredoxin: Structure, Dynamics and Electrostatics of Reduced Pig Glutaredoxin and its Mutants. *J. Mol. Biol. 372*, 798−816.
(26) Gane, P. J., Freedman, R. B., and Warwicker, J. (1995) A Molecular Model for the Redox Potential Difference Between Thioredoxin and DsbA, Based on Electrostatic Calculations. *J. Mol. Biol. 249*, 376−387.
(27) Mössner, E., Huber-Wunderlich, M., and Glockshuber, R. (1998) Characterization of *Escherichia coli* thioredoxin variants mimicking the active-sites of other thiol/disulfide oxidoreductases. *Protein Sci. 7*, 1233−1244.
(28) Jeng, M. F., Holmgren, A., and Dyson, H. J. (1995) Proton Sharing between Cysteine Thiols in *Escherichia coli*Thioredoxin: Implications for the Mechanism of Protein Disulfide Reduction. *Biochemistry 34*, 10101−10105.
(29) Guddat, L. W., Bardwell, J. C. A., Glockshuber, R., Huber-Wunderlich, M., Zander, T., and Martin, J. L. (1997) Stuctural analysis of three His32 mutants of DsbA: Support for an electrostatic role of His32 in DsbA stability. *Protein Sci. 6*, 1893−1900.
(30) Nordstrand, K., Åslund, F., Meunier, S., Holmgren, A., Otting, G., and Berndt, K. D. (1999) Direct NMR observation of the Cys-14 thiol proton of reduced *Escherichia coli* glutaredoxin-3 supports the presence of an active site thiol-thiolate hydrogen bond. *FEBS Lett. 449*, 196−200.
(31) Dillet, V., and Bashford, D. (1998) Calculations of Electrostatic Interactions and pK_as in the Active Site of *Escherichia coli* Thioredoxin. *Biochemistry 37*, 10298−10306.
(32) Moutevelis, E., and Warwicker, J. (2004) Prediction of pK_a and redox properties in the thioredoxin superfamily. *Protein Sci. 13*, 2744−2752.
(33) Roos, G., Loverix, S., and Geerlings, P. (2006) Origin of the pK_a perturbation of Nterminal cysteine in α- and 3(10)-helices: A computational DFT study. *J. Phys. Chem. B 110*, 557−562.
(34) Carvalho, A. T. P., Fernandes, P. A., and Ramos, M. J. (2006) Theoretical Study of the Unusual Protonation Properties of the Active Site Cysteines in Thioredoxin. *J. Phys. Chem. B 110*, 5758−5761.
(35) Porat, A., Lillig, C. H., Johansson, C., Fernandes, A. P., Nilsson, L., Holmgren, A., and Beckwith, J. (2007) The Reducing Activity of Glutaredoxin 3 Towards Cytoplasmic Substrate Proteins is Restricted by Methionine 43. *Biochemistry 46*, 3366−3377.
(36) Lewin, A., Crow, A., Hodson, C. T. C., Hederstedt, L., and Le Brun, N. E. (2008) Effects of substitutions in the CXXC active-site motif of the extracytoplasmic thioredoxin ResA. *Biochem. J. 414*, 81−91.
(37) Clore, G. M., and Gronenborn, A. M. (1998) New methods of structure refinement for macromolecular structure determination by NMR. *Proc. Natl. Acad. Sci. U.S.A. 95*, 5891−5898.
(38) Lee, M. R., and Kollman, P. A. (2001) Free-Energy Calculations Highlight Differences in Accuracy between X-ray and NMR Structures and Add value to Protein Structure Prediction. *Structure 9*, 905−916.
(39) Spronk, C. A. E. M., Linge, J. P., Hilbers, C. W., and Vuistera, G. W. (2002) Improving the quality of protein structures derived by NMR spectroscopy. *J. Biomol. NMR 22*, 281−289.
(40) Nabuurs, S. B., Nederveen, A. J., Vranken, W., Doreleijers, J. F., Bonvin, A. M. J. J., Vuister, G. W., Vriend, G., and Spronk, C. A. E. M. (2004) DRESS: A Database of REfined Solution NMR Structures. *Proteins 55*, 483−486.
(41) Powers, N., and Jensen, J. H. (2006) Chemically accurate protein structures: Validation of protein NMR structures by comparison of measured and predicted pK_a values. *J. Biomol. NMR 35*, 39−51.
(42) Xia, B., Tsui, V., Case, D. A., Dyson, H. J., and Wright, P. E. (2002) Comparison of protein solution structures refined by molecular dynamics simulation in vacuum, with a generalized Born model, and with explicit water. *J. Biomol. NMR 22*, 317−331.

(43) Linge, J. P., Williams, M. A., Spronk, C. A. E. M., Bonvin, A. M. J. J., and Nilges, M. (2003) Refinement of Protein Structures in Explicit Solvent. *Proteins 50*, 496−506.
(44) Linge, L. P., and Nilges, M. (1999) Influence of non-bonded parameters on the quality of NMR structures: A new force-field for NMR structure calculation. *J. Biomol. NMR 13*, 51−59.
(45) Roos, G., Foloppe, N., Van Laer, K., Wyns, L., Nilsson, L., Geerlings, P., and Messens, J. (2009) How Thioredoxin Dissociates Its Mixed Disulfide. *PLoS Comput. Biol. 5*, e1000461.
(46) MacKerell, A. D., Jr., Bashford, D., Bellott, M., Dunbrack, R. L., Jr., Evanseck, J. D., Field, M. J., Fisher, S., Gao, J., Guo, H., Ha, S., Joseph-McCarthy, D., Kuchnir, L., Kuczera, K., Lau, F. T. K., Mattos, C., Michnick, S., Ngo, T., Nguyen, D. T., Prodhom, B., Reiher, W. E., III, Roux, B., Schlenkrich, M., Smith, J. C., Stote, R., Straub, J., Watanabe, M., Wiórkiewicz-Kuczera, J., Yin, D., and Karplus, M. (1998) All-Atom Empirical Potential for Molecular Modeling and Dynamics Studies of Proteins. *J. Phys. Chem. B 102*, 3586−3616.
(47) Brooks, B., Brooks, C. L., Mackerell, A. D., Nilsson, L., Petrella, R. J., Roux, B., Won, Y., Archontis, G., Bartels, C., Boresch, S., Caflisch, A., Caves, L., Cui, Q., Dinner, A. R., Feig, M., Fischer, S., Gao, J., Hodoscek, M., Im, W., Kuczera, K., Lazaridis, T., Ma, J., Ovchinnikov, V., Paci, E., Pastor, R. W., Post, C. B., Pu, J. Z., Schaefer, M., Tidor, B., Venable, R. M., Woodcock, H. L., Wu, X., Yang, W., York, D. M., and Karplus, M. (2009) CHARMM: The Biomolecular Simulation Program. *J. Comput. Chem. 30*, 1545−1614.
(48) Steinbach, P. J., and Brooks, B. R. (1994) New Spherical-Cutoff Methods for Long-Ranges Forces in Macromolecular Simulation. *J. Comput. Chem. 15*, 667−683.
(49) Norberg, J., and Nilsson, L. (2000) On the truncation of long-range electrostatic interactions in DNA. *Biophys. J. 79*, 1537−1553.
(50) Cheatham, T. E., and Kollman, P. A. (2000) Molecular Dynamics Simulation of Nucleic Acids. *Annu. Rev. Phys. Chem. 51*, 435−471.
(51) Beck, D. A. C., Armen, R. S., and Daggett, V. (2005) Cutoff Size Need Not Strongly Influence Molecular Dynamics Results for Solvated Polypeptides. *Biochemistry 44*, 609−616.
(52) http://www.chemcomp.com/.
(53) Jorgensen, W. L., Chandrasekhar, J., Madura, J. D., Impey, R. W., and Klein, M. L. (1983) Comparison of simple potential functions for simulating liquid water. *J. Chem. Phys. 79*, 926−935.
(54) Ryckaert, J. P., Ciccotti, G., and Berendsen, H. J. C. (1977) Numerical integration of the Cartesian equations of motion of a system with constraints: Molecular dynamics of n-alkanes. *J. Comput. Phys. 23*, 327−341.
(55) Madura, J. D., Briggs, J. M., Wade, R. C., Davis, M. E., Luty, B. A., Ilin, A., Antosiewicz, J., Gilson, M. K., Bagheri, B., Scott, L. R., and McCammon, J. A. (1995) Electrostatics and diffusion of molecules in solution: Simulations with the University of Houston Brownian Dynamics program. *J. Comput. Phys. Commun. 91*, 57−95.
(56) Demchuk, E., and Wade, R. C. (1996) Improving the Continuum Dielectric Approach to Calculating pK_as of Ionizable Groups in Proteins. *J. Phys. Chem. 100*, 17373−17387.
(57) Raquet, X., Lounnas, V., Lamotte-Brasseur, J., Frere, J. M., and Wade, R. C. (1997) pK_a Calculations for Class A β-Lactamases: Methodological and Mechanistic Implications. *Biophys. J. 73*, 2416−2426.
(58) Gilson, M. K., Sharp, K. A., and Honig, B. H. (1987) Calculating the Electrostatic Potential of Molecules in Solution: Method and Error Assessment. *J. Comput. Chem. 9*, 327−335.
(59) Gilson, M. K. (1993) Multiple-Site Titration and Molecular Modeling: Two Rapid Methods for Computing Energies and Forces for Ionizable Groups in Proteins. *Proteins 15*, 266−282.
(60) Markley, J. L., Bax, A., Arata, Y., Hilbers, C. W., Kaptein, R., Sykes, B. D., Wright, P. E., and Wüthrich, K. (1998) Recommendations for the Presentation of NMR Structures of Proteins and Nucleic Acids. *J. Mol. Biol. 280*, 933−952.
(61) Donohue, J. (1969) On N-H···S hydrogen bonds. *J. Mol. Biol. 45*, 231−235.
(62) Adman, E., Watenpaugh, K. D., and Jensen, L. H. (1975) NH···S Hydrogen bonds in *Peptococcus aerogenes* ferredoxin, *Clostridium pasteurianum* rubredoxin, and *Chromatium* high potential iron protein. *Proc. Natl. Acad. Sci. U.S.A. 72*, 4854−4858.
(63) Gregoret, L.-M., Rader, S. D., Fletterick, R. J., and Cohen, F. E. (1991) Hydrogen Bonds Involving Sulfur Atoms in Proteins. *Proteins 9*, 99−107.
(64) Kerr, K. A., and Ashmore, J. P. (1975) A Neutron Diffraction Study of L-Cysteine. *Acta Crystallogr. B31*, 2022−2026.
(65) Allen, F. H., Bird, C. M., Rowland, R. S., and Raithby, P. R. (1997) Hydrogen-Bond Acceptor and Donor Properties of Divalent Sulfur (Y-S-Z and R-S-H). *Acta Crystallogr. B53*, 696−701.
(66) Studier, F. W. (2005) Protein Production by Auto-Induction in High-Density Shaking Cultures. *Protein Expression Purif. 41*, 207−234.
(67) Vlamis-Gardikas, A., Åslund, F., Spyrou, G., Bergman, T., and Holmgren, A. (1997) Cloning, Overexpression, and Characterization of Glutaredoxin 2, an Atypical Glutaredoxin from *Escherichia coli*. *J. Biol. Chem. 272*, 11236−11243.
(68) Benesch, R. E., and Benesch, R. (1955) The Acid Strength of the -SH Group in Cysteine and Related Compounds. *J. Am. Chem. Soc. 77*, 5877−5881.
(69) Polgar, L. (1974) Spectrophotometric determination of mercaptide ion, an activated form of SH-group in thiol enzymes. *FEBS Lett. 38*, 187−190.
(70) Ellman, G. L. (1959) Tissue sulfhydryl groups. *Arch. Biochem. Biophys. 82*, 70−77.
(71) Kerr, K. A., and Ashmore, J. P. (1973) Structure and conformation of orthorhombic L-cysteine. *Acta Crystallogr. B29*, 2124−2127.
(72) Foloppe, N., Chen, I., Davis, B., Hold, A., Morley, D., and Howes, R. (2004) A structure-based strategy to identify new molecular scaffolds targeting the bacterial ribosomal A-site. *Bioorg. Med. Chem. 12*, 935−947.
(73) Li, H., Robertson, A. D., and Jensen, J. H. (2005) Very Fast Empirical Prediction and Rationalization of Protein pK_a Values. *Proteins 61*, 704−721.
(74) Thurlkill, R. L., Grimsley, G. R., Scholtz, J. M., and Pace, C. N. (2006) pK values of the ionizable groups of proteins. *Protein Sci. 15*, 1214−1218.
(75) Shekhter, T., Metanis, N., Dawson, P. E., and Keinan, E. (2010) A residue outside the active site CXXC motif regulates the catalytic efficiency of glutaredoxin 3. *Mol. BioSyst. 6*, 241−248.
(76) Berardi, M. J., and Bushweller, J. H. (1999) Binding Specificity and Mechanistic Insight into Glutaredoxin-catalysed Protein Disulfide Reduction. *J. Mol. Biol. 292*, 151−161.
(77) Li, Y., Hu, Y., Zhang, X., Xu, H., Lescop, E., Xia, B., and Jin, C. (2007) Conformational Fluctuations Coupled to the Thiol-Disulfide Transfer between Thioredoxin and Arsenate Reductase in *Bacillus subtilis*. *J. Biol. Chem. 282*, 11078−11083.
(78) Singha, N. C., Vlamis-Gardikas, A., and Holmgren, A. (2003) Real-time Kinetics of the Interaction between the Two Subunits, *Escherichia coli* Thioredoxin and Gene 5 Protein of Phage T7 DNA Polymerase. *J. Biol. Chem. 278*, 21421−21428.
(79) Takahashi, N., and Creighton, T. E. (1996) On the Reactivity and Ionization of the Active Site Cysteine Residues of *Escherichia coli* Thioredoxin. *Biochemistry 35*, 8342−8353.
(80) Forman-Kay, J. D., Clore, G. M., Wingfield, P. T., and Gronenborn, A. M. (1991) High-resolution three-dimentional structure of reduced recombinant human thioredoxin in solution. *Biochemistry 30*, 2685−2698.